Nature and Origin of Stable Metallic State in Organic Charge-Transfer Complexes of Bis(ethylenedioxy)tetrathiafulvalene

Sachio Horiuchi,*,† Hideki Yamochi,† Gunzi Saito,*,† Ken-ichi Sakaguchi,‡ and Masami Kusunoki‡

Contribution from the Division of Chemistry, Graduate School of Science, Kyoto University, Sakyo-ku, Kyoto 606-01, Japan, and Institute for Protein Research, Osaka University, Suita, Osaka 565, Japan

Received February 6, 1996[⊗]

Abstract: The complex formation of bis(ethylenedioxy)tetrathiafulvalene (BEDO-TTF) with 29 organic electron acceptors and six organic anions yielded 37 charge-transfer (CT) complexes, about three-quarters of which exhibited metallic behavior. The BEDO-TTF molecule proves to be an excellent source for stable metals irrespective of the structure, shape, size, and electron affinity of counter components. The crystal structure of metallic BEDO-TTF complexes indicates a strong aggregation of donor molecules into a two-dimensional (2D) layered structure by the aid of both intermolecular C−H···O and side-by-side heteroatom contacts. Band calculations based on an extended Hückel method demonstrate that the sulfur atoms of the BEDO-TTF molecule are dominant for 2D intermolecular overlap. The resulting 2D electronic bands with large band width serve to stabilize the metallic state even at low temperatures. A comparison between the structural properties of complexes of BEDO-TTF and those of its sulfur analog BEDT-TTF (BEDT-TTF = bis(ethylenedithio)tetrathiafulvalene) demonstrates that the oxygen atoms of the BEDO-TTF molecule not only enhance the intermolecular S··S atomic contacts due to its small size, but also determine donor packing through multiple weak hydrogen bondings. The nicely combined roles of these heteroatoms are the origins of the strongly stabilized metallic state in BEDO-TTF complexes without aid of heavier selenium and/or further addition of sulfur atoms on TTF moiety.

Introduction

Extensive work has been carried out in the design of organic metals and superconductors of charge-transfer (CT) complexes.[1,2] Such complexes are classifiable into two main groups. The first is a donor (D)−acceptor (A) type complex derived from closed-shell organic electron donor and acceptor molecules, as exemplified by the first organic metal, TTF-TCNQ[3] (for this and other chemical abbreviations in text, see the ref 4). The second group is comprised of radical salts which are made up of the radical ion of an organic donor or acceptor molecule and a closed-shell counterion.

To obtain organic metals based on planar π-molecules, it is necessary that donor and/or acceptor molecules form a uniform segregated columnar structure and have a partial CT ground state.[5] Particularly in formation of DA-type complexes, relative strength of the components plays a critical role in the conducting properties.[6] Since these materials consist of planar molecules, their electronic structures are essentially low dimensional, which causes a metal−insulator transition driven by charge- or spin-density wave (CDW or SDW) instability. To stabilize the metallic state, various chemical modifications have been made to the π-molecules, either by introducing weak disorder into the crystals or by increasing the dimensionality of their electronic structures. The latter modification, e.g., substitution of the sulfur atoms for heavier atoms (Se and Te)[7] and/or addition of further peripheral chalcogen atoms to the TTF skeleton,[8] has yielded fruitful results. The most successful examples are TMTSF and BEDT-TTF, both of which have produced a number of superconductors and low-temperature organic metals.

Most organic superconductors are obtained as radical salts.[9] The superconducting transition temperature (T_c) has markedly

† Kyoto University.

‡ Osaka University.

[⊗] Abstract published in *Advance ACS Abstracts,* August 1, 1996.

(1) Cowan, D. O. In *Proc. 4th. Int. Kyoto Conf. on New Aspects of Organic Chemistry*; Yoshida, Z., Shiba, T., Oshiro, Y., Eds.; Prentice-Hall: Englewood Cliffs, NJ, 1992.

(2) Saito, G. In *Metal-Insulator Transition Revisited*; Edwards, P. P., Rao, C. N. R., Eds.; Taylor & Francis: London, UK, 1995; p 231.

(3) Ferraris, J. P.; Cowan, D. O.; Walatka, V. V.; Perlstein, J. H. *J. Am. Chem. Soc.* **1973**, *95*, 948.

(4) Abbreviations for chemicals in text: TTF, tetrathiafulvalene; BEDO-TTF, bis(ethylenedioxy)tetrathiafulvalene; BEDT-TTF, bis(ethylenedithio)-tetrathiafulvalene; TMTSF, tetramethyltetraselenafulvalene; TSF, tetraselenafulvalene; HMTTF, hexamethylenetetrathiafulvalene; TMTTF, tetramethyltetrathiafulvalene; TTC_1-TTF, tetra(methylthio)tetrathiafulvalene; BEDT-TSF, bis(ethylenedithio)tetraselenafulvalene; BDT-TTP, 2,5-bis(1′,3′-mercapto-2′-ylidene)-1,3,4,6-tetrathiapentalene; DTEDT, 2-(1,3-mercapto-2-ylidene)-5-(2-ethanediylidene-1,3-dithiole)-1,3,4,6-tetrathiapentalene; TCNQ, 7,7,8,8-tetracyano-*p*-quinodimethane; F_4TCNQ, tetrafluoro−7,7,8,8-tetracyano-*p*-quinodimethane; F_2TCNQ, 2,5-difluoro−7,7,8,8-tetracyano-*p*-quinodimethane; FTCNQ, 2-fluoro 7,7,8,8-tetracyano-*p*-quinodimethane; Me_2-TCNQ, 2,5-dimethyl−7,7,8,8-tetracyano-*p*-quinodimethane; Et_2TCNQ, 2,5-diethyl−7,7,8,8-tetracyano-*p*-quinodimethane; $(MeO)_2$TCNQ, 2,5-dimethoxy-7,7,8,8-tetracyano-*p*-quinodimethane; C_{10}TCNQ, 2-decyl-7,7,8,8-tetracyano-*p*-quinodimethane; C_{14}TCNQ, 2-tetradecyl-7,7,8,8-tetracyano-*p*-quinodimethane; DHBTCNQ, dihydrobarreleno-7,7,8,8-tetracyano-*p*-quinodimethane; THBTCNQ, tetrahydrobarreleno-7,7,8,8-tetracyano-*p*-quinodimethane; BTDA-TCNQ, bis-1,2,5-thiadiazolo-7,7,8,8-tetracyano-*p*-quinodimethane; DDQ, 2,3-dichloro-5,6-dicyano-*p*-benzoquinone; DBDQ, 2,3-dibromo-5,6-dicyano-*p*-benzoquinone; QF_4, 2,3,5,6-tetrafluoro-*p*-benzoquinone; QCl_4, 2,3,5,6-tetrachloro-*p*-benzoquinone; QBr_4, 2,3,5,6-tetrabromo-*p*-benzoquinone; $QCl_2(OH)_2$, 2,5-dichloro-3,6-dihydroxy-*p*-benzoquinone; $QBr_2(OH)_2$, 2,5-dibromo-3,6-dihydroxy-*p*-benzoquinone; $Q(OH)_2$, 2,5-dihydroxy-*p*-benzoquinone; DCNQ, 2,3-dicyano-1,4-naphthoquinone; HCBD, hexacyano-1,3-butadiene; TCNE, tetracyanoethylene; DTENF, 9-(dicyanomethylene)-2,4,5,7-tetranitrofluorene; DTNF, 9-(dicyanomethylene)-2,4,7-trinitrofluorene; TENF, 2,4,5,7-tetranitrofluoren-9-one; TNF, 2,4,7-trinitrofluoren-9-one; TNBP, 3,3′,5,5′-tetranitrobiphenyl-4,4′-diol; DNBP, 4,4′-dinitrobiphenyl; CF^-, cyanoform anion; HCP^{2-}, tris(dicyanomethylene)cyclopropandiide; SQA^{2-}, squarate, PCA^-, 1,1,2,3,3-pentacyanopropenide; PIC^-, picrate; $HCTMM^{2-}$, hexacyanotrimethylenemethanediide; TBA^+, tetra(*n*-butyl)ammonium; TPA^+, tetra(*n*-propyl)ammonium; THF, tetrahydrofuran; AN, acetonitrile; PhCN, benzonitrile; TCE, 1,1,2-trichloroethane.

S0002-7863(96)00393-9 CCC: $12.00

Chart 1. BEDO-TTF and BEDT-TTF

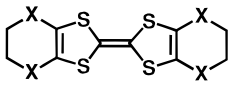

X=O: BEDO-TTF
X=S: BEDT-TTF

increased as the dimensionality of the electronic structure has been raised from quasi-one-dimensional (1D) (e.g. $(TMTSF)_2X$ salts[9a]) to two-dimensional (2D) (e.g. κ-$(BEDT\text{-}TTF)_2X$ salts[2,9b−e,10]). At the same time, the above structural requirement for organic metal was modified; not only columnar, but also a layered structure of D or A molecules can enable the metallic state when intermolecular interactions are sufficient. For example, the κ-type salts reveal the 2D layers assembled of the dimers of donor molecules instead of columns. BEDT-TTF derivatives thus seem to be good candidates for higher dimensional conductors of the DA-type, as well as for superconductors. In fact, 2D donor layers and 1D acceptor columns appear in triclinic (BEDT-TTF) (TCNQ) complex.[11] However, among 20 DA-type BEDT-TTF complexes currently known[11,12] only three are metals: (BEDT-TTF) (FTCNQ), (BEDT-TTF) $(F_2TCNQ)_x(TCNQ)_{1-x}$ ($x = 0.5$),[12j] and the triclinic form of TCNQ complex.

As one of the various kinds of BEDT-TTF analogs designed with the aim of increasing T_c of superconductivity, the oxygen analog donor, BEDO-TTF (Chart 1) was synthesized in 1989 by Suzuki et al.[13] Since then, its cation radical salts have been prepared with about 30 inorganic anions.[14] Only three of these are semiconducting, and most of the rests are metals, including two superconductors with T_c of about 1 K.[15] Further, we have recently reported that this donor molecule easily yields a number of metallic complexes with organic acceptors and wide metallic temperature region.[16] It is not sufficiently understood why there is such a remarkable contrast between the abilities of two analogous donors to produce metallic complexes.

The primary goal of this paper is to elucidate the physical and structural properties and the electronic state of BEDO-TTF CT complexes in order to characterize their unusual accessibility to formation of organic metal, and to offer a deeper understanding of their origin.

Experimental Section

General. Melting points were not corrected. Cyclic voltammetric measurements were performed in 0.1 M solutions of $(TBA)BF_4$ in AN with Pt working and counter electrodes vs SCE (saturated calomel electrode). Optical measurements, for infrared and near-infrared regions (400−7800 cm^{-1}) were carried out using the KBr disk method with Perkin-Elmer 1600 Series FT-IR (resolution 4 cm^{-1}) and for near-infrared, visible, and ultraviolet (UV−vis−near-IR) regions (3800−42000 cm^{-1}) on SHIMADZU UV-3100 spectrometer. Electronic absorption spectra were also measured in AN solution. IR spectra (650−4000 cm^{-1}) with higher resolution (0.5 cm^{-1}) were recorded on Nicolet Magna-IR 750 spectrometer. Crystal densities were determined using the floating method with a mixture of carbon tetrachloride and 1,2-dibromoethane. DC conductivities were measured with either a standard four- or two-probe technique, using gold paint to attach gold wires to the samples. For powdered samples, measurements were performed on compressed pellets which were cut to form an orthorhombic shape.

Preparation of BEDO-TTF Complexes. BEDO-TTF was synthesized according to the literature[13] and recrystallized twice from cyclohexane. DDQ, TCNQ, TCNE, QCl_4, QF_4, $QCl_2(OH)_2$, $QBr_2(OH)_2$, $Q(OH)_2$, TNF, and K(CF) were purchased. We synthesized the following organic acceptors and electrolytes according to the literatures: HCBD,[17a] F_4TCNQ,[17b] DBDQ,[17c] F_2TCNQ,[12j] FTCNQ,[12j] DTENF,[17d] DCNQ,[17e] Me_2TCNQ,[17f] Et_2TCNQ,[17f] $(MeO)_2TCNQ$,[17f] QBr_4,[17g] BTDA-TCNQ,[17h] DTNF,[17i] TENF,[17j] TNBP,[17k] DNBP,[17l] $(TPA)_2HCTMM$,[17m] $K_2(SQA)(H_2O)$,[17n] (TBA)PIC,[17o] (TBA)PCA,[17p] and $(TBA)_2HCP$.[17q] $(TBA)_2HCTMM$ was prepared from Ba(HCTMM)[17m] and (TBA)Br. All these acceptors and electrolytes were purified by recrystallization and/or gradient sublimation and identified by elemental analysis. DHBTCNQ and THBTCNQ were kindly supplied by Prof. K. Nakasuji, and $C_{10}TCNQ$ and $C_{14}TCNQ$, by Prof. T. Nakamura. Chart 2 shows the chemical structures of organic acceptors and anions used

(5) (a) Garito, A. F.; Heeger, A. J. *Acc. Chem. Res*. **1974**, *7*, 232. (b) Torrance, J. B. *Acc. Chem. Res.* **1979**, *12*, 79.

(6) Saito, G.; Ferraris, J. P. *Bull. Chem. Soc. Jpn*. **1980**, *53*, 2141 and the references cited therein.

(7) (a) Bloch, A. N.; Cowan, D. O.; Bechgaard, K.; Pyle, R. E.; Banks, R. H.; Poehler, T. O. *Phys. Rev. Lett*. **1975**, *34*, 1561. (b) Mays, M. D.; McCullough, R. D.; Cowan, D. O.; Poehler, T. O.; Bryden, W. A.; Kistenmacher, T. J. *Solid State Commun*. **1988**, *65*, 1089.

(8) Saito, G.; Enoki, T.; Toriumi, K.; Inokuchi, H. *Solid State Commun*. **1982**, *42*, 557.

(9) (a) Jerome, D.; Schulz, H. J. *Adv. Phys*. **1982**, *31*, 299. (b) Ishiguro, T.; Yamaji, K. *Organic Superconductors*; Springer Ser. Solid State Sci., 88; Springer: Berlin, 1990. (c) Williams, J. M.; Ferraro, J. R.; Thorn, R. J.; Carlson, K. D.; Geiser, U.; Wang, H. H.; Kini, A. M.; Whangbo, M.-H. *Organic Superconductors* (*including Fullerenes*): *Synthesis, Structure, Properties, and Theory*; Prentice Hall: Englewoods Cliffs, NJ, 1992. (d) Saito, G. *Phosphorus, Sulfur Silicon Relat. Elem*. **1992**, *67*, 345. (e) Saito, G. In *New Materials*; Joshi, S. K., Tsuruta, T., Rao, C. N. R., Nagakura, S., Eds.; Narosa Publishing House: New Delhi, India, 1992, p 127.

(10) (a) Urayama, H.; Yamochi, H.; Saito, G.; Nozawa, K.; Sugano, T.; Kinoshita, M.; Sato, S.; Oshima, K.; Kawamoto, A.; Tanaka, J. *Chem. Lett*. **1988**, 55. (b) Kini, A. M.; Geiser, U.; Wang, H. H.; Carlson, K. D.; Williams, J. M.; Kwok, W. K.; Vandervoort, K. G.; Thompson, J. E.; Stupka, D. L.; Jung, D.; Whangbo, M.-H. *Inorg. Chem*. **1990**, *29*, 2555. (c) Williams, J. M.; Kini, A. M.; Wang, H. H.; Carlson, K. D.; Geiser, U.; Montgomery, L. K.; Pyrka, G. J.; Watkins, D. M.; Kommers, J. M.; Boryschuk, S. J.; Crouch, A. V. S.; Kwok, W. K.; Schirber, J. E.; Overmyer, D. L.; Jung, D.; Whangbo, M.-H. *Inorg. Chem*. **1990**, *29*, 3272. (d) Komatsu, T.; Nakamura, T.; Matsukawa, N.; Yamochi, H.; Saito, G.; Ito, H.; Ishiguro, T.; Kusunoki, M.; Sakaguchi, K. *Solid State Commun*. **1991**, *80*, 843.

(11) Mori, T.; Inokuchi, H. *Solid State Commun*. **1986**, *59*, 355.

(12) (a) Mizuno, M.; Garito, A. F.; Cava, M. P. *J. Chem. Soc., Chem. Commun*. **1978**, 18. (b) Saito, G.; Hayashi, H.; Enoki, T.; Inokuchi, H. *Mol. Cryst. Liq. Cryst*. **1985**, *120*, 341. (c) Yamashita, Y.; Suzuki, T.; Saito, G.; Mukai, T. *J. Chem. Soc., Chem. Commun*. **1986**, 1489. (d) Mori, T.; Inokuchi, H. *Bull. Chem. Soc. Jpn*. **1987**, *60*, 402. (e) Yui, K.; Aso, Y.; Otsubo, T.; Ogura, F. *Bull. Chem. Soc. Jpn*. **1989**, *62*, 1539. (f) Yui, K.; Ishida, H.; Aso, Y.; Otsubo, T.; Ogura, F.; Kawamoto, A.; Tanaka, J. *Bull. Chem. Soc. Jpn*. **1989**, *62*, 1547. (g) Suzuki, T.; Yamashita, Y.; Kabuto, C.; Miyashi, T. *J. Chem. Soc., Chem. Commun*. **1989**, 1102. (h) Izuoka, A.; Tachikawa, T.; Sugawara, T.; Suzuki, Y.; Konno, M.; Saito, Y.; Shinohara, H. *J. Chem. Soc., Chem. Commun*. **1992**, 1472. (i) Günther, E.; Hünig, S.; Schütz, J.-U.; Langohr, U.; Rieder, H.; Söderholm, S.; Werner, H.-P.; Peters, K.; Schnering, H. G.; Lindner, H. J. *Chem. Ber*. **1992**, *125*, 1919. (j) Hasegawa, T.; Itoh, N.; Inukai, K.; Kagoshima, S.; Mochida, T.; Izuoka, A.; Sugawara, T.; Iwasa, Y.; Sugiura, S. Private communication.

(13) (a) Suzuki, T.; Yamochi, H.; Srdanov, G.; Hinkelmann, K.; Wudl, F. *J. Am. Chem. Soc*. **1989**, *111*, 3108. (b) Suzuki, T.; Yamochi, H.; Isotalo, H.; Fite, C.; Kasmai, H.; Liou, K.; Srdanov, G.; Wudl, F.; Coppens, P.; Maly, K.; Frost-Jensen, A. *Synth. Met*. **1991**, *41*−*43*, 2225.

(14) (a) Wudl, F.; Yamochi, H.; Suzuki, T.; Isotalo, H.; Fite, C.; Kasmai, H.; Liou, K.; Srdanov, G.; Coppens, P.; Maly, K.; Frost-Jensen, A. *J. Am. Chem. Soc*. **1990**, *112*, 2461. (b) Wudl, F.; Yamochi, H.; Suzuki, T.; Isotalo, H.; Fite, C.; Liou, K.; Kasmai, H.; Srdanov, G. In *The Physics and Chemistry of Organic Superconductors*; Springer, Proceeding in Physics, Vol. 51; Saito, G., Kagoshima, S., Eds.; Springer-Verlag: Berlin, 1990; p 358. (c) Beno, M. A.; Wang, H. H.; Carlson, K. D.; Kini, A. M.; Frankenbach, G. M.; Ferraro, J. R.; Larson, N.; McCabe, G. D.; Thompson, J. E.; Purnama, C.; Vashion, M.; Williams, J. M. *Mol. Cryst. Liq. Cryst*. **1990**, *181*, 145. (d) Yamochi, H.; Nakamura, T.; Saito, G.; Kikuchi, T.; Sato, S.; Nozawa, K.; Kinoshita, M.; Sugano, T.; Wudl, F. *Synth. Met*. **1991**, *41*−*43*, 1741. (e) Schweitzer, D.; Kahlich, S.; Heinen, I.; Lan, S. E.; Nuber, B.; Keller, H. J.; Winzer, K.; Helberg, H. W. *Synth. Met*. **1993**, *55*−*57*, 2827. (f) Saito, G.; Yoshida, K.; Shibata, M.; Yamochi, H.; Kojima, N.; Kusunoki, M.; Sakaguchi, K. *Synth. Met*. **1995**, *70*, 1205.

(15) (a) Beno, M. A.; Wang, H. H.; Kini, A. M.; Carlson, K. D.; Geiser, U.; Kwok, W. K.; Thompson, J. E.; Williams, J. M.; Ren, J.; Whangbo, M.-H. *Inorg. Chem*. **1990**, *29*, 1599. (b) Kahlich, S.; Schweitzer, D.; Heinen, I.; Lan, S. E.; Nuber, B.; Keller, H. J.; Winzer, K.; Helberg, H. W. *Solid State Commun*. **1991**, *80*, 191.

(16) (a) Yamochi, H.; Horiuchi, S.; Saito, G.; Kusunoki, M.; Sakaguchi, K.; Kikuchi, T.; Sato, S. *Synth. Met*. **1993**, *55*−*57*, 2096. (b) Yamochi, H.; Horiuchi, S.; Saito, G. *Phosphorus, Sulfur Silicon Relat. Elem*. **1992**, *67*, 305.

Chart 2. Acceptor Molecules and Organic Anions Used for Preparation of BEDO-TTF Complexes

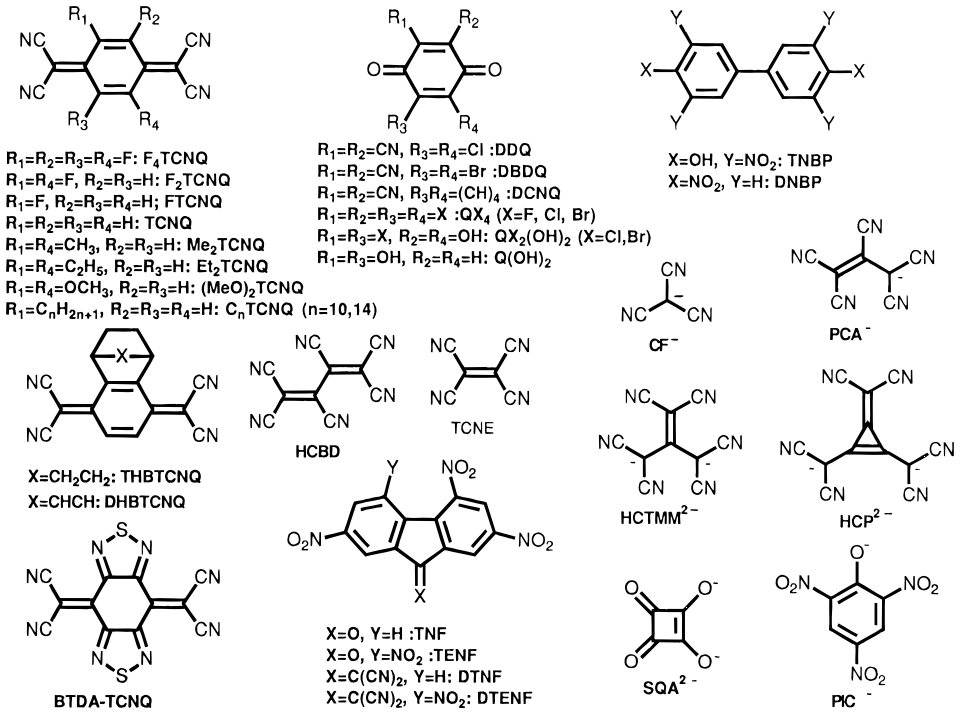

Table 1. Typical Conditions of Preparation of BEDO-TTF Radical Salts

salts (D = BEDO-TTF)	donor, mg	supporting electrolytes, mg	solvents, mL	current, μA	yield, mg
$D_5(HCTMM)(PhCN)_2$	10.8	$(TPA)_2HCTMM$, 68.5	PhCN, 18	0.2	5.4
$D_4(HCTMM)(TCE)_2$	10.4	$(TBA)_2HCTMM$, 76.6	TCE, 16; EtOH 2	0.7	6.3
$D_{10}(CF)_4(H_2O)_3$	19.6	K(CF), 50.8; 18-crown-6, 116.1	PhCN, 18; H_2O 2 drops	0.2	3.6
$D_4(SQA)(H_2O)_6$	12.0	$K_2(SQA)(H_2O)$, 52.5; 18-crown-6, 96.9	PhCN, 18; H_2O 2 drops	0.1	1.6
$D_6(PIC)_3(TCE)$	13.7	(TBA)PIC, 45.6	TCE, 18	0.1	1.1
$D_8(PCA)_4(H_2O)$	16.6	(TBA)PCA, 54.4	PhCN, 18; H_2O 2 drops	0.4	4.4
$D_5(HCP)(PhCN)_{0.2}$	25.2	$(TBA)_2HCP$, 37.4	PhCN, 17; EtOH 1	0.1	1.3

in this work. CT complexes with organic acceptors were prepared by mixing two hot solutions of each component. The complexes, precipitated out upon cooling, were collected by filtration, washed with the same solvent as used for the preparation, and dried in vacuo. The solvents used were THF for F_4TCNQ and TCNQ complexes, benzene for DTENF one, and AN for complexes with other acceptors. Using AN, F_4TCNQ yielded a complex different than that obtained from THF. Our attempts to obtain large single crystals of metallic DA-type complexes by slow cooling, recrystallization, or diffusion method were unsuccessful.

BEDO-TTF radical salts with six kinds of organic anions were prepared by electrocrystallization under constant current, typical conditions of which are given in Table 1. Two kinds of HCTMM salts were obtained from different electrolytes and solvents.

Table 2 summarizes their stoichiometry, appearance, and decomposition points. All BEDO-TTF complexes will be represented by their numbers in the table hereafter. The stoichiometries of **27**, **29**, **31**, **33**, **34**, and **37** were determined by X-ray analysis (see below), crystal densities, and elemental analysis, and those of other complexes were determined solely by elemental analysis. Although the stoichiometry of complex **8** remains ambiguous due to the large difference between observed and calculated contents, those of other BEDO-TTF complexes were determined satisfactorily (±0.3% for C, H, N, O, S, and halogen).

Crystal Structure Determinations. Crystal structure was determined for six of the CT complexes (numbers **27**, **29**, **31**, **33**, **34**, and **37**). Intensity data were collected on the RIGAKU AFC-4 or AFC-5 automatic four-circle diffractometer at room temperature. The structures were solved by direct methods using the SHELXS-86 program.[18] The structure refinements were performed by block-diagonal least-squares method (UNICS)[18] for **27** and **31**, and full matrix least-squares method (SHELX-76)[18] for **29**, **33**, **34**, and **37**. Table 3 summarizes the parameters for crystals, data collection, and refinement. Parameters were refined by adopting anisotropic temperature factors for non-hydrogen atoms of the donor molecules in all crystals and for acceptor molecules in **27** and **29**. The positions were determined by differential synthesis and following refinement with isotropic temperature factors for all hydrogen atoms in **27** and those of the OH groups of TNBP in **29**. Other hydrogen atoms in **29** were refined with isotropic temperature factors under a fixed C−H bond length of 1.08 Å. The positions of hydrogen atoms of the donor molecules were calculated for **31**, **33**, **34**, and **37**.[19] The refined and calculated atomic parameters are

(17) (a) Webster, O. W. *J. Am. Chem. Soc.* **1964**, *86*, 2898. (b) Wheland, R. C.; Martin, E. L. *J. Org. Chem.* **1975**, *40*, 3101. (c) Thiele, J.; Günther, F. *Justus Liebigs Ann. Chem.* **1906**, *349*, 45. (d) Hutzinger, O.; Haecock, R. A.; Macneil, J. D.; Frei, R. W. *J. Chromatogr.* **1972**, *68*, 173. (e) Reynolds, G. A.; Vanallen, J. A. *J. Org. Chem.* **1964**, *29*, 3591. (f) Uno, M.; Seto, K.; Masuda, M.; Ueda, W.; Takahashi, S. *Tetrahedron Lett.* **1985**, *26*, 1553. (g) Torrey, H. A.; Hunter, W. H. *J. Am. Chem. Soc.* **1912**, *34*, 702. (h) Yamashita, Y.; Suzuki, T.; Mukai, T.; Saito, G. *J. Chem. Soc., Chem. Commun.* **1985**, 1044. (i) Mukherjee, T. K.; Levasseuer, L. A. *J. Org. Chem.* **1965**, *30*, 644. (j) Ray, F. E.; Francis, W. C. *J. Org. Chem.* **1943**, *8*, 52. (k) Kunze, E. *Chem. Ber.* **1888**, *21*, 3331. (l) Gull, H. C.; Turner, E. E. *J. Chem. Soc.* **1929**, 491. (m) Middelton, W. J.; Little, E. L.; Coffman, D. D.; Engelhardt, V. A. *J. Am. Chem. Soc.* **1958**, *80*, 2795. (n) Park, J. D.; Cohen, S.; Lacher, J. R. *J. Am. Chem. Soc.* **1962**, *84*, 2919. (o) Birr, W. *Z. Phys. Chem.* **1931**, *153*, 1. (p) Yamochi, H.; Tsuji, T.; Saito, G.; Suzuki, T.; Miyashi, T.; Kabuto, C. *Synth. Met.* **1988**, *27*, A479 and references cited therein. (q) Fukunaga, T. *J. Am. Chem. Soc.* **1976**, *98*, 610.

(18) (a) Sheldrick, G. M. SHELXS-86, Program for Crystal Structure Determination and SHELX-76, Program for Crystal Structure Determination, Univ. of Göttingen, Federal Republic of Germany. (b) Ashida, T. HBLS-V (UNICS), 1967.

Table 2. Compositions, Appearances, Decomposition Temperatures of BEDO-TTF Complexes

	composition (D:A or X:Solv)	appearance	D_p, °C		composition (D:A or X:Solv)	appearance	D_p, °C
Acceptor				Acceptor			
1 HCBD	2:1	dark green powder	204−209	**16** Me_2TCNQ	9:5:1AN	dark blue powder	186−189
2 F_4TCNQ	1:1	dark green powder	196−199	**17** Et_2TCNQ	2:1	black powder	190−195
3 F_4TCNQ	9:5:4THF	greenish brown powder	194−198	**18** $(MeO)_2TCNQ$	2:1	dark bluish green powder	182−185
4 DDQ	5:3:1AN	dark brown powder	162−166	**19** QCl_4	2:1	dark green powder	162−164
5 DBDQ	11:7:1AN	reddish brown powder	166−168	**20** QF_4	11:5:6H_2O	black powder	151−156
6 F_2TCNQ	2:1	dark bluish powder	192−196	**21** QBr_4	9:5:1H_2O	greenish brown powder	151−154
7 FTCNQ	4:2:1AN	dark greenish powder	186−189	**22** BTDA-TCNQ	7:4	black powder	197−199
8 TCNE	2:1[a]	greenish brown powder	157−162	**23** DTNF	2:1:1AN	black powder	138−141
9 DTENF	2:1	black powder	188−191	**24** $QBr_2(OH)_2$	2:1	reddish brown powder	158−163
10 TCNQ	1:1	black powder	206−208	**25** $QCl_2(OH)_2$	2:1	black powder	151−155
11 DCNQ	2:1	dark brown powder	164−172	**26** TENF	1:1	black powder	174−176
12 $C_{10}TCNQ$	10:4:1H_2O	dark green powder	138−142	**27** $Q(OH)_2$	1:2	black plates	125−134
13 $C_{14}TCNQ$	9:4:2H_2O	black powder	131−133	**28** TNF	1:1	reddish brown powder	178−182
14 DHBTCNQ	2:1	black powder	112−115	**29** TNBP	1:1	black plates	170−178
15 THBTCNQ	2:1	dark green powder	138−141	**30** DNBP	1:1	bluish gray powder	199−202
Anion (X)				Anion (X)			
31 HCTMM	5:1:2PhCN	black plates	165−172	**35** PIC	6:3:1TCE	dark green needles	175−181
32 HCTMM	4:1:2TCE	black needles	154−161	**36** PCA	8:4:1H_2O	brownish green powder	177−183
33 CF	10:4:3H_2O	black needles	110−117	**37** HCP	5:1:0.2PhCN	black needles	260−267
34 SQA	4:1:6H_2O	black needles	153−159				

[a] The stoichiometry of **8** is still ambiguous because of the large differences between the observed and calculated content of the elemental analysis.

Table 3. Crystal Data, Data Collection, and Reduction Parameters

	31	**33**	**34**	**37**	**27**	**29**
anion or acceptor (A)	HCTMM	CF	SQA	HCP	$Q(OH)_2$	TNBP
BEDO-TTF:A:solvent	5:1:2PhCN	1:0.4:0.3H_2O	2:0.5:3H_2O	1:0.2:0.04PhCN	1:2	1:1
formula weight	2012.65	361.88	750.97	370.21	600.64	686.65
space group	triclinic, $P\bar{1}$	triclinic, $P\bar{1}$	triclinic, $P\bar{1}$	monoclinic, $P2_1/c$	triclinic, $P\bar{1}$	monoclinic, $C2/c$
crystal dimensions, mm^3	0.67 × 0.20 × 0.04	0.45 × 0.10 × 0.05	0.67 × 0.20 × 0.04	0.30 × 0.25 × 0.03	0.4 × 0.3 × 0.2	0.75 × 0.75 × 0.05
a, Å	10.855(2)	5.342(2)	10.752(2)	17.075(2)	9.312(3)	15.220(3)
b, Å	19.224(3)	17.225(4)	16.517(4)	4.085(4)	9.785(2)	11.118(2)
c, Å	10.286(2)	4.0307(7)	4.0971(6)	20.462(4)	7.364(2)	16.426(4)
α, deg	91.76(2)	102.85(2)	87.35(1)		94.68(3)	
β, deg	107.22(2)	98.59(2)	82.01(2)	96.46(2)	96.99(3)	109.96(2)
γ, deg	91.77(2)	93.47(2)	79.74(2)		116.89(2)	
V, $Å^3$	2047.3(7)	335.8(2)	708.9(2)	1418(1)	586.9(3)	2613(1)
Z	1	1	1	4	1	4
d_{cald}, g cm^{-3}	1.63	1.69	1.76	1.71	1.70	1.75
d_{obs}, g cm^{-3}	1.62	1.70	1.76	1.72	1.69	1.73
radiation	Mo Kα	Cu Kα	Mo Kα	Mo Kα	Mo Kα	Mo Kα
diffractometer	AFC-5	AFC-5	AFC-4	AFC-4	AFC-4	AFC-4
scan mode	$2\theta - \omega$	ω	ω	ω	$2\theta - \omega$	ω
$2\theta_{max}$	65	125	60	60	60	60
no. of intensity measd	14 990	1369	6257	4951	3660	6341
criterion for obsd reflections	$F > 3\sigma(F)$	$F > 3\sigma(F)$	$F > 3\sigma(F)$	$F > 3\sigma(F)$	$F > 3\sigma(F)$	$F > 3\sigma(F)$
no. of independent obsd reflections	4150	997	3180	2102	2743	3085
no. of refined parameters	407	82	187	235	205	236
R	0.127	0.100	0.050	0.084	0.037	0.074
R_w[a]				0.077[b]	0.044[c]	

[a] Quantity minimized $\sum w(F_o - F_c)^2$. [b] $w = a/[\sigma^2 + b|F_o|^2]$; $a = 1.7471$, $b = 0.000934$. [c] $w = 1/[\sigma^2 + a|F_o|^2]$; $a = -0.01538$, $b = 0.00133$.

deposited as supporting information. Details specific to each structure determination are given in the following.

$(BEDO\text{-}TTF)_5(HCTMM)(PhCN)_2$ (31). The cell was determined with the aid of oscillation and Weissenberg photographs. Severe disorder of counter components prevented the determination of their positions.[16a]

$(BEDO\text{-}TTF)_{10}(CF)_4(H_2O)_3$ (33). The positions of counter molecules could not be determined because the obtained cell was too small for them. No superlattices were detected, even by oscillation or Weissenberg photograph, suggesting that anion and water molecules were too randomly disordered to reveal their periodicity.

$(BEDO\text{-}TTF)_4(SQA)(H_2O)_6$ (34). The unit cell parameters, especially parameter *c*, were not enough to accommodate the squarate molecule (vide infra). Oscillation and Weissenberg photographs revealed a supercell of (a, $-b + c$, $-2c$) whose corresponding reflections were, however, too weak to determine the definite structure; only 903 and 1521 out of 5882 independent reflections satisfied the criterions, $F > 3\sigma(F)$ and $F > 2\sigma(F)$, respectively. The structure described here is thus the averaged one. (A similar situation has also been reported in the case of $(BEDO\text{-}TTF)_2ClO_4$.[14c]) The non-hydrogen atoms of the water and squarate were refined with isotropic temperature factors. The occupancy factors of the squarate and two water molecules were fixed to $^1/_2$, while those of the other two water molecules were unity.

$(BEDO\text{-}TTF)_5(HCP)(PhCN)_{0.2}$ (37).[16a] The cell parameter *b* described in this paper is too short to accommodate the anion and solvent molecules. The precise cell is (a, $5b$, c), but weakness of the reflections from its corresponding supercell prevented our solving the definite structure; only 314 and 595 out of 2908 independent reflections ($2\theta < 60°$, Cu Kα) satisfied the criterions, $F > 3\sigma(F)$ and $F > 2\sigma(F)$, respectively. Thus, the crystal structure given here is also the averaged one. In the refinement of the donor molecule, the differential Fourier

(19) The sp^3 configuration with the C−H bond length of 1.0 Å is assumed for ethylene groups in the donor molecules.

map presented the peaks corresponding to anions along the $x = 0$ plane. The peak pattern was accounted for by the assumption that two HCP anions were located on the 2-fold screw axis in the period of 5*b*. Therefore, the occupancy factor was fixed to $^1/_5$ for the anion atoms. Their positional and isotropic thermal parameters were refined with their bond lengths fixed correspondent to HCP dianion.[20] Although the Fourier map showed very weak remaining peaks related to the solvent molecule in the openings of the anion layer, this molecule was too diluted in the crystal to allow the refinement of its positions.

(BEDO-TTF)[Q(OH)$_2$]$_2$ (27). During the X-ray measurement, the surface of this black crystal gradually decomposed to form an orange solid. To avoid this, the crystal was coated with silicon grease.

Band Electronic Structure Calculations. The tight-binding band calculations were based on the extended Hückel method.[21] The semiempirical parameters for Slater-type atomic orbitals were taken from refs 21b,c. The intermolecular transfer integrals (t) were assumed to be proportional to the corresponding overlap integrals (S) of the highest occupied molecular orbital (HOMO) of BEDO-TTF ($t = -ES$, $E = 10$ eV). In the band calculations of the I_3, ClO_4, $AuBr_2$, $Cu_2(NCS)_3$, ReO_4, and Cl salts, we employed the positional parameters of the non-hydrogen atoms of BEDO-TTF taken from the literatures,[14a,c,e,15a] as well as those of the hydrogen atoms which, although not available in the above literatures, were obtainable from our calculations.[19]

Results and Discussion

Electron-Donating Property of BEDO-TTF. The difference between ionization potential of a donor and electron affinity of an acceptor is essential for determining the ionicity, and thus the conducting properties, of the CT complex.[5b,6] According to the photoelectron spectroscopy (PES) in the gas phase,[22] both the first vertical and the adiabatic ionization potentials (I_P(D) and I_P^{ad}(D)) increase in the following order: BEDO-TTF (6.46 and 6.12 eV, respectively) < TTF (6.70 and 6.26 eV) ≈ BEDT-TTF (6.7 and 6.30 eV). The order of the last two molecules is, however, different from that of the previously reported I_P^{ad}(D) values (BEDT-TTF, 6.21 eV; TTF, 6.4 eV).[23] Since the PES spectrum of BEDT-TTF in ref 22 is more resolved than that in ref 23, we utilize the ionization potentials of the former for use in the following discussion.

The first oxidation (or reduction) potential $E_{1/2}^1$(D) (or $E_{1/2}^1$(A)) is related to the adiabatic ionization potential (or electron affinity). Our cyclic voltammetry measurements indicate that BEDO-TTF (0.43 V vs SCE) is stronger than BEDT-TTF (0.53 V), but weaker than TTF (0.37 V) in donating ability, a finding that agrees with reported measurements.[22] However, this order is different from the results for I_P^{ad}(D). In Figure 1a, we plot I_P^{ad}(D) vs $E_{1/2}^1$(D) for eight TTF system donors, obtaining the linear relation

$$I_P^{ad}(D) = eE_{1/2}^1(D) + 5.76 \text{ eV} \quad (1)$$

except for the nonsubstituted donors (TTF and TSF). While the deviation of TTF may be ascribed to its different solvation energy,[23] the pronounced deviation of TSF requires the reexamination of its I_P^{ad}(D) value.

The difference (ΔE) between the $E_{1/2}^1$(D) and the second oxidation potential ($E_{1/2}^2$(D)) is presented in the following order: TTF (0.38 V) > BEDO-TTF (0.26 V) ∼ BEDT-TTF (0.25 V). This is indicative of the reduction of on-site Coulomb energy from TTF to BEDO-TTF and BEDT-TTF.

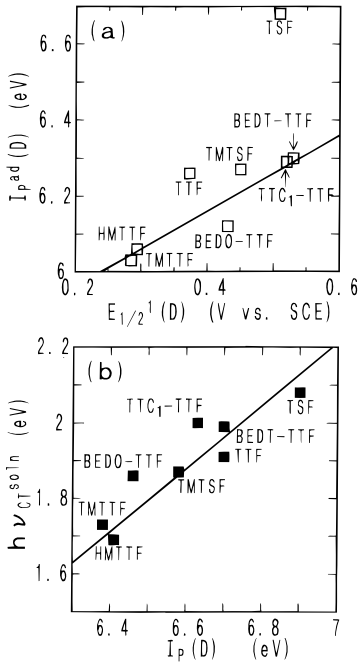

Figure 1. (a) Correlation between the adiabatic ionization potential (I_P^{ad}(D))[22,23] and the first oxidation potential ($E_{1/2}^1$(D)) for the TTF derivatives. The solid line represents eq 1). (b) Correlation between the CT transition energy of the s-trinitrobenzene complexes in chloroform ($h\nu_{CT}^{soln}$) and the first vertical ionization potential (I_P(D))[22,23] of the TTF derivatives. The solid line is the least squares fit (eq 3).

We also measured the CT transition energy ($h\nu_{CT}^{soln}$) of the complex with *s*-trinitrobenzene in chloroform in order to compare donating ability. The $h\nu_{CT}^{soln}$ is usually approximated as

$$h\nu_{CT}^{soln} = a[I_P(D) - E_A(A)] - C \quad (2)$$

where E_A(A) is the vertical electron affinity of an acceptor molecule (A), C the Coulomb attractive energy of a D−A pair, and a the constant close to the unity.[24] The plotting of $h\nu_{CT}^{soln}$ vs I_P(D) values (Figure 1b) gives a line by least-squares fit as

$$h\nu_{CT}^{soln} = aI_P(D) - 3.62 \text{ eV} \quad (3)$$

where $a = 0.836$. On the basis of the eq 3, the difference of the estimated I_P(D) values of BEDO-TTF ($h\nu_{CT}^{soln} = 1.86$ eV) and BEDT-TTF (1.99 eV) is 0.16 eV, in good agreement with that from the PES measurement (0.2 eV).

All these measurements consistently indicate that the ionization potential of BEDO-TTF is lower than that of BEDT-TTF by 0.1−0.2 eV. Therefore, one can expect metallic BEDO-TTF complexes from combination with weaker acceptors than would be possible for BEDT-TTF.

Conductivity. Table 4 summarizes the conducting properties of BEDO-TTF complexes, as well as the $E_{1/2}^1$(A) values, where σ_{rt} is the conductivity at room temperature of the metal (M) or semiconductor (S), $T_{\sigma_{max}}$ the temperature at which conductivity reaches the maximum (σ_{max}) for the metal, and E_a the activation energy of the semiconductor. They show several characteristic features, as follows: (i) many have unusual stoichiometries rather than the conventional 1:1, 2:1 or 1:2; (ii) 28 out of 37 complexes were found to be metallic; (iii) metallic behavior

(20) Miller, J. S.; Ward, M. D.; Zhang, J. H.; Reiff, W. M. *Inorg. Chem.* **1990**, *29*, 4063.
(21) (a) Mori, T.; Kobayashi, A.; Sasaki, Y.; Kobayashi, H.; Saito, G.; Inokuchi, H. *Bull. Chem. Soc. Jpn.* **1984**, *57*, 627. (b) Summerville, R. H.; Hoffmann, R. *J. Am. Chem. Soc.* **1976**, *98*, 7240. (c) Berlinsky, A. J.; Carolan, J. F.; Weiler, L. *Solid State Commun.* **1974**, *15*, 795.
(22) Lichtenberger, D. L.; Johnston, R. L.; Hinkelmann, K.; Suzuki, T.; Wudl, F. *J. Am. Chem. Soc.* **1990**, *112*, 3302.
(23) Sato, N.; Saito, G.; Inokuchi, H. *Chem. Phys.* **1983**, *76*, 79 and references cited therein.
(24) Foster, R. *Organic Charge Transfer Complexes*; Academic Press: London, 1969.

Table 4. Conducting Properties of BEDO-TTF Complexes and the Redox Potentials of Their Counter Components

	complex[a]	$E_{1/2}^1$(A) (V vs SCE)[b]	conductivity σ_{rt}, S cm^{-1} [c]		$T_{\sigma_{max}}$, K[d]	σ_{max}/σ_{rt}	E_a, eV
			DA-Type Complexes				
1	D_2(HCBD)	+0.72	1.0×10^2	(M)	13	5.9	
2	D(F_4TCNQ)	+0.60	7.9×10^{-8}	(S)*			0.40
3	$D_9(F_4TCNQ)_5(THF)_4$	+0.60	1.4×10	(M)	100	1.8	
4	$D_5(DDQ)_3$(AN)	+0.56	4.7×10	(M)	15	4.0	
5	$D_{11}(DBDQ)_7$(AN)	+0.54	3.6×10	(M)	72	2.2	
6	$D_2(F_2TCNQ)$	+0.41	1.0×10^2	(M)	11	12	
7	$D_4(FTCNQ)_2$(AN)	+0.32	6.5×10	(M)	5	19	
8	D_2(TCNE)	+0.29	6.9×10	(M)	13	7.9	
9	D_2(DTENF)	+0.23	1.8×10	(M)	94	1.8	
10	D(TCNQ)	+0.22	8.1×10^{-2}	(S)			0.066
11	D_2(DCNQ)	+0.21	1.1×10	(M)	48	5.3	
12	$D_{10}(C_{10}TCNQ)_4(H_2O)$	+0.21	7.3	(M)	136	1.4	
13	$D_9(C_{14}TCNQ)_4(H_2O)_2$	+0.21	9.9×10^{-1}	(S)			0.026 (90−200 K)
14	D_2(DHBTCNQ)	+0.18	1.1×10^2	(M)	13	5.2	
15	D_2(THBTCNQ)	+0.16	3.3×10	(M)	18	3.6	
16	$D_9(Me_2TCNQ)_5$(AN)	+0.15	3.6×10	(M)	18	4.5	
17	$D_2(Et_2TCNQ)$	+0.15	1.4×10^2	(M)	9	4.9	
18	D_2[$(MeO)_2$TCNQ]	+0.05	4.7×10	(M)	5**	15	
19	$D_2(QCl_4)$	+0.05	7.6×10	(M)	16	8.1	
20	$D_{11}(QF_4)_5(H_2O)_6$	+0.04	6.8×10	(M)	20	4.2	
21	$D_9(QBr_4)_5(H_2O)$	+0.04	3.6×10	(M)	77	2.0	
22	D_7(BTDA-TCNQ)$_4$	+0.03	6.1×10	(M)	164	1.1	
23	D_2(DTNF)(AN)	+0.02	6.5×10	(M)	8	6.0	
24	D_2[$QBr_2(OH)_2$]	−0.12[1]	1.4×10^2	(M)	16	5.7	
25	D_2[$QCl_2(OH)_2$]	−0.13[1]	1.7×10^2	(M)	11	4.2	
26	D(TENF)	−0.14	5.6×10^{-10}	(S)*			0.45
27	D[$Q(OH)_2$]$_2$	−0.38[1]	10^{-7}	(S)*,+			0.35
28	D(TNF)	−0.43	2.5×10^{-10}	(S)*			0.50
29	D(TNBP)	−0.56[1]	3.5×10^{-8}	(S)*,+			0.35
30	D(DNBP)	−0.98	4.5×10^{-10}	(S)*			0.47
			Radical Salts				
31	D_5(HCTMM)$(PhCN)_2$	+0.96[2,3]	2.8×10 (//a+2c)	$(M)^+$	5**	40	
			7.0×10 (//2a−c)	$(M)^+$	5**	30	
			1.4×10^2	(M)	14	7.3	
32	D_4(HCTMM)$(TCE)_2$	+0.96[2,3]	1.1×10^2	$(M)^+$	235	1.1	
33	$D_{10}(CF)_4(H_2O)_3$	+1.32[2,5]	1.1×10^2 (//c)	$(M)^+$	1.3**	19	
34	$D_4(SQA)(H_2O)_6$		1.7×10^2 (//c)	$(M)^+$	1.4**	46	
35	$D_6(PIC)_3$(TCE)	>1.4[4]	2×10^2	$(M)^+$	1.4**	49	
36	$D_8(PCA)_4(H_2O)$	>1.4[4]	3.3×10	$(M)^+$	16	5.2	
37	$D_5(HCP)(PhCN)_{0.2}$	+0.42[3]	1.8×10 (//c)	$(S)^+$			0.10
		+1.21[4]	4.1×10^{-1} (//b)	$(S)^+$			0.05

[a] D = BEDO-TTF. [b] The first half-wave reduction potential: (1) irreversible (cathodic peak potential), (2) irreversible (anodic peak potential), (3) TBA salt ($X^{2-} \rightleftarrows X^-$), (4) TBA salt ($X^- \rightleftarrows X$), (5) K salt ($X^- \rightleftarrows X$). [c] (M), metal; (S), semiconductor; rt, room temperature (285K); ($^+$), measured on single crystal; (*), 2 probe. [d] (**) the lowest temperature we measured.

was observed, even on the compressed pellet, for 23 complexes which were obtained only as powder; (iv) about 70% of the metals retain metallic behavior down to temperature of 20 K or even lower, although below these temperatures they do not show a distinct metal−insulator transition; (v) the room temperature conductivity is not very high (≤200 S cm^{-1}); (vi) the conductivity enhancement is poor even on the single crystal ($\sigma_{max}/\sigma_{rt} < 50$); (vii) the acceptor molecules in the metals are rather fertile in the shape, size, and strength.

The conductivity of the metallic CF (**33**), SQA (**34**), PIC (**35**), and the two kinds of HCTMM (**31**, **32**) radical salts was measured on the single crystals. The HCTMM salts, which were obtained from different solvents (PhCN, TCE), exhibit differences not only in their stoichiometry but also in their conducting properties; 5:1:2 PhCN salt (**31**) is a low-temperature organic metal while a metal−insulator transition with $T_{\sigma_{max}} = 235$ K was observed for the 4:1:2 TCE salt (**32**) (Figure 2a). **33**−**35** are metallic down to the lowest temperature measured (1.3−1.4 K). The σ_{rt} values are 30−200 S cm^{-1} for the above four low-temperature organic metals. The resistivities are simply proportional to T^α ($1 \le \alpha \le 2$), a relation typically seen in low-dimensional organic metals. The conductivity enhancement is only 20−50. The disorder of the anions, as will be seen in the crystal structures of **31** and **33**, is considered to be one reason for the high residual resistivity.

We found metallic behavior on the compressed pellet of the DA-type complexes and PCA salt (**36**) which were obtained only as powder (Table 4). For example, the temperature-dependent resistivities of the C_{10}TCNQ (**12**), $(MeO)_2$TCNQ (**18**), and QCl_4 (**19**) complexes are shown in Figure 2b. The 2:1 complex **18** remains metallic down to 5 K, accompanied by a conductivity 15 times that of σ_{rt} (47 S cm^{-1}). **19** is also metallic to low temperatures (16 K), below which its resistivity increases slightly. Similarly, in metals **1**, **3**−**9**, **11**−**12**, **14**−**17**, **20**−**25**, and **36** resistivities minimize on cooling, but below the cooled temperature exhibit neither the rapid increase characteristic of the Peierls or SDW phase transition, nor the Arrhenius-type temperature dependence; their resistivities at 4−5 K are at most on the same order of the room temperature values. Among these metals, the TCNQ derivative with bulky alkyl chain yielded the least conducting complex **12** ($\sigma_{rt} = 7.3$ S cm^{-1}), with resistivity increasing gradually below 135 K, but remaining low (0.1 S cm^{-1}) even at 1.6 K (Figure 2b). The poor conductivity and high $T_{\sigma_{max}}$ may be ascribed to the bulkiness of the acceptor (see below).

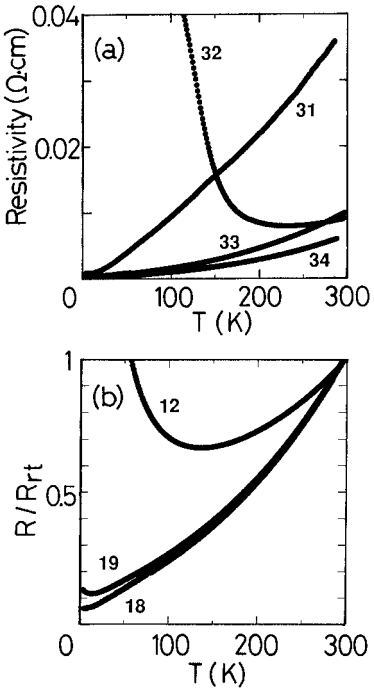

Figure 2. Temperature dependence of the resistivity: (a) On single crystals for (BEDO-TTF)$_5$(HCTMM)(PhCN)$_2$ (**31**) (//a + 2c), (BEDO-TTF)$_4$(HCTMM)(TCE)$_2$ (**32**), (BEDO-TTF)$_{10}$(CF)$_4$(H$_2$O)$_3$ (**33**) (//c), and (BEDO-TTF)$_4$(SQA)(H$_2$O)$_6$ (**34**) (//c); (b) on the compressed pellets for (BEDO-TTF)$_{10}$(C$_{10}$TCNQ)$_4$(H$_2$O) (**12**), (BEDO-TTF)$_2$[(MeO)$_2$-TCNQ] (**18**), and (BEDO-TTF)$_2$(QCl$_4$) (**19**).

The intrinsic temperature-dependent resistivities measured on the compressed pellet of the microcrystalline remain ambiguous because they usually include the resistance due to interparticle contact.[25] By grinding crystals of **31**, we were able to actually compare conducting properties on the single crystal and compressed pellet. The compressed sample shows comparable σ_{rt} ($\sim$100 S cm^{-1}), but high $T_{\sigma_{max}}$ (14 K) and low conductivity enhancement (σ_{14K}/σ_{rt} = 7.3) as compared to results on the single crystal ($T_{\sigma_{max}} \leq$ 5 K, σ_{5K}/σ_{rt} = 20−30). Below 14 K, the conductivity of the pellet decreases slightly (σ_{4K}/σ_{14K} = 0.91). On the basis of these facts, the intrinsic conductivity of the powdered sample should remain metallic down to at least $T_{\sigma_{max}}$ observed on the pellet. Including the results on single crystal, 20 complexes are essentially metallic to the low temperature (<20 K), which indicates BEDO-TTF is an excellent source for stable metals. For the other TTF-based conductors, stable metallic states are realized by enhancing the interstack interactions with the aid of heavier Se atoms and/or by extending π-conjugation system with further introduced sulfur atoms, as exemplified by the complexes of BEDT-TSF[26] and BDT-TTP.[27] The BEDO-TTF molecule, however, yields stable metals without these chemical modifications.

Semiconducting behavior was observed in eight DA-type complexes and one radical salt. Complexes **10**, **13**, and **37** show relatively high σ_{rt} and small E_a ($\leq$0.10 eV). Compared with metallic **12**, σ_{rt} is 8 times decreased for **13** with its further bulky alkyl chain, which seems to inhibit metallic conduction. Highly resistive F$_4$TCNQ complex (**2**) (σ_{rt} = 7.9 × 10^{-8} S cm^{-1}, E_a = 0.40 eV) was obtained from AN as a 1:1 stoichiometry, which differs from that of metallic **3** (9:5:4THF). Five weak acceptor molecules ($E_{1/2}^1$(A) $\leq$ −0.14 V) produced highly resistive semiconductors (**26**−**30**) due to the ground state of neutral CT.

We should also note that BEDO-TTF DA-type complexes exhibit the following unique stoichiometry characteristics: (i) 1:1 complexes are less conducting and mainly obtained as neutral complexes (**26**, **28**−**30**); (ii) only **27** shows 1:2, having a strong hydrogen-bond network among the acceptor molecules (see below); (iii) the highly conductive complexes contain the donor in excess, with donor/acceptor (D/A) ratios ranging from 1.6 (**5**) to 2.5 (**12**); (iv) about one-half of the metallic (**3**−**5**, **12**, **16**, and **20**−**22**) and highly conducting (**13**) complexes are non-stoichiometric, and most of these contain solvent molecules. Therefore, disorder can be expected in their crystals.

It is important to emphasize that, unlike BEDT-TTF, BEDO-TTF easily provides stable organic metals with D/A > 1 and a wide variety of acceptor molecules of different size, shape, and strength. In the following we will examine the electronic states of those complexes to clarify their conducting properties.

IR Spectrum and Degree of Charge Transfer. Infrared spectrum is useful for identifying the ionicity of the ground state of the CT complex;[28] degree of CT, particularly, can be estimated by utilizing those specific vibrations the frequencies of which are sensitive to the ionicity of the molecule.[29] Table 5 lists the frequencies of the CN stretching modes of the counter components and the $b_{1u}\nu_{31}$ mode of BEDO-TTF. First, we estimate the degree of CT (γ) for some BEDO-TTF complexes, on the basis of the vibrations of the acceptors.

Two (BEDO-TTF)-F$_4$TCNQ complexes show contrastive features in their optical spectra: the vibrational bands are distinct for the insulator **2**, whereas those for metallic **3** are obscured by the CT electronic band. It has been previously reported that the two C═C stretching vibrational bands (1551 cm^{-1} ($b_{1u}\nu_{19}$) and 1598 cm^{-1} ($b_{2u}\nu_{33}$) for F$_4$TCNQ^0) show red shifts by 51 and 62 cm^{-1}, respectively, on ionization to (F$_4$TCNQ)$^{-1}$ (Figure 3a,b).[30] The spectrum of **2** shows absorption at 1500 and 1536 cm^{-1}, corresponding to (F$_4$TCNQ)$^{-1}$, but shows no bands ascribable to the F$_4$TCNQ species in the partial or neutral CT around 1540−1600 cm^{-1} (Figure 3c). **2** is thus regarded as completely ionic since D/A = 1. The CN stretching frequencies (2228 cm^{-1} ($b_{1u}\nu_{18}$) and 2214 cm^{-1} ($b_{2u}\nu_{32}$) for F$_4$TCNQ^0, which shift by 34 and 42 cm^{-1} upon ionization, respectively) correspond to (F$_4$TCNQ)$^{-1}$ for **3** (2198, 2177 cm^{-1}) as well as for **2** (2195, 2170 cm^{-1}).

For other BEDO-TTF complexes with strong acceptors, such as HCBD (**1**) and DDQ (**4**), CN stretching frequencies are characterized according to their completely ionized acceptor molecules.[31,32] An analogous conclusion can be made for **5** (ν_{CN} = 2216 cm^{-1}), based on comparison with DBDQ^0 (2230 cm^{-1}) and (TEA)DBDQ (2214 cm^{-1}).[33] The monoanionic acceptor molecules in **1** and **3**−**5** demand the partially oxidized BEDO-TTF molecule because D/A > 1. Accordingly, in this text we define the γ of BEDO-TTF complexes as the charge on the donor molecules. The respective γ of **1**, **2**, **3**, **4**, and **5** are deduced from their D/A ratios to be 0.5, 1, 0.56, 0.60, and 0.64.

(25) Coleman, L. B. *Rev. Sci. Instrum.* **1978**, *49*, 58.
(26) (a) Kato, R.; Kobayashi, H.; Kobayashi, A. *Synth. Met.* **1991**, *41*, 2093. (b) Kobayashi, A.; Kato, R.; Naito, T.; Kobayashi, H. *Synth. Met.* **1993**, *56*, 2078. (c) Montgomery, L. K.; Burgin, T.; Huffman, J. C.; Carlson, K. D.; Dudek, J. D.; Yaconi, G. A.; Megna, L. A.; Mobley, P. R.; Kwok, W. K.; Williams, J. M.; Schirber, J. E.; Overmyer, D. L.; Ren, J.; Rovira, C.; Whangbo, M.-H. *Synth. Met.* **1993**, *56*, 2090.
(27) Misaki, Y.; Fujiwara, H.; Yamabe, T.; Mori, T.; Mori, H.; Tanaka, S. *Chem. Lett.* **1994**, 1653.
(28) Matsunaga, Y. *Nature* **1965**, *205*, 72.
(29) Chappell, J. S.; Bloch, A. N.; Bryden, W. A.; Maxfield, M.; Poehler, T. O.; Cowan, D. O. *J. Am. Chem. Soc.* **1981**, *103*, 2442.
(30) Meneghetti, M.; Pecile, C. *J. Chem. Phys.* **1986**, *84*, 4149.
(31) (a) Miller, J. S.; Zhang, J. H.; Reiff, W. M. *J. Am. Chem. Soc.* **1987**, *109*, 4584. (b) Miller, J. S.; Calabrese, J. C.; Dixon, D. A. *J. Phys. Chem. Soc.* **1991**, *95*, 3139.
(32) Miller, J. S.; Krusic, P. J.; Dixon, D. A.; Reiff, W. M.; Zhang, J. H.; Anderson, E. C.; Epstein, A. J. *J. Am. Chem. Soc.* **1986**, *108*, 4459.
(33) (TEA)DBDQ was prepared by mixing DBDQ and (TEA)I in analogous way of the preparation of (TEA)DDQ.[32]

Table 5. Optical Properties of BEDO-TTF and Its Complexes

		vibrational spectra,[b] cm^{-1}		electronic spectra,[b] 10^3 cm^{-1}		
	complex[a]	$b_{1u}\nu_{31}$[c]	ν_{CN}	$h\nu_{CT}$	UV−vis	average charge on BEDO-TTF:[d] γ
	BEDO-TTF	1015.4			20, 26,* 29,* 32	0.00
			DA-Type Complexes			
1	D_2(HCBD)	1004.0	2220, 2188, 2170	2.6	14, 16,* 22, 30*	0.50
2	D(F_4TCNQ)	1000.2	2195, 2170	6.7*	9.3,* 12, 13, 20,* 26	1.0
3	$D_9(F_4TCNQ)_5(THF)_4$	1005.7	2198, 2177	1.8	8,* 11, 13,* 14,* 26	0.56
4	$D_5(DDQ)_3$(AN)	1002.3	2215	2.0	12, 20, 31	0.60
5	$D_{11}(DBDQ)_7$(AN)	1001.9	2216	2.0	12, 19	0.64
6	$D_2(F_2TCNQ)$	1006	2194, 2172	2.5	7, 12,* 14, 25, 27	
7	$D_4(FTCNQ)_2$(AN)	1004	2188	2.9	12, 13, 16, 27	
8	D_2(TCNE)	1003	2144	2.0	13, 32	
9	D_2(DTENF)	1006	2183, 2158	2.4	8,* 12, 17, 32*	
10	D(TCNQ)	1011.0	2001,* 2194, 2179	4.5	10, 12,* 16,* 20, 28	**
		1003.3	2160			
11	D_2(DCNQ)	1002	2193	3.0	13, 20, 32*	
12	$D_{10}(D_{10}TCNQ)_4(H_2O)$	1006	2178	2.5	12, 13, 16, 28	
13	$D_9(C_{14}TCNQ)_4(H_2O)_2$	1005	2176, 2159	4.0	12, 13, 15,* 27	
14	D_2(DHBTCNQ)	1007	2172	2.2	12, 13, 16,* 29	
15	D_2(THBTCNQ)	1007	2158	2.0	12, 13, 17, 29	
16	$D_9(Me_2TCNQ)_5$(AN)	1007	2188	2.4	12, 13,* 17, 27	
17	$D_2(Et_2TCNQ)$	1006	2183	2.0	12, 13,* 17, 26	
18	$D_2[(MeO)_2TCNQ]$	1008	2188	2.5	12,* 14, 17, 26, 30*	
19	$D_2(QCl_4)$	1006		3.5	13, 24, 34	
20	$D_{11}(QF_4)_5(H_2O)_6$	1006		2.2	12, 32	
21	$D_9(QBr_4)_5(H_2O)$	1006		3.5	14, 23, 33	
22	D_7(BTDA-TCNQ)$_4$	1006	2191	2.5	9, 13, 16,* 22,* 32	
23	D_2(DTNF)(AN)	1007	2179	1.8	8,* 13, 32	
24	$D_2[QBr_2(OH)_2]$	1003		2.1	13, 20,* 32	
25	$D_2[QCl_2(OH)_2]$	1003		2.5	12, 18,* 31	
26	D(TENF)	1010		7.4*	12, 19	
27	$D[Q(OH)_2]_2$	1010		8*	11, 18, 35	
28	D(TNF)	1014		10.3	13, 19,* 35	
29	D(TNBP)	1012		15*	19,* 38	
30	D(DNBP)	1012		14*	17, 32	
			Radical Salts			
31	$D_5(HCTMM)(PhCN)_2$	1006.2	2229, 2176, 2162	2.2	13, 29	0.40
32	$D_4(HCTMM)(TCE)_2$	1004.0	2189, 2177, 2163*	2.3	13, 30	0.50
33	$D_{10}(CF)_4(H_2O)_3$	1005.2	2158	2.5	12, 28,* 32	0.40
34	$D_4(SQA)(H_2O)_6$	1006.2		2.1	13	0.50
35	$D_6(PIC)_3$(TCE)	1001.4		3.0	13, 23,* 27	0.50
36	$D_8(PCA)_4(H_2O)$	1003.8	2198	3.0	13, 26	0.50
37	$D_5(HCP)(PhCN)_{0.2}$	1006.0	2185, 2165	3.0	12, 31	0.40

[a] D = BEDO-TTF. [b] On KBr disk; (*) shoulder. [c] The results on the higher resolution (0.5 cm^{-1}) measurements are represented by larger fingers than the usual ones (4 cm^{-1}). [d] Determined from the charge on the counter component and stoichiometry; (**) charge separation (see text).

Among the BEDO-TTF radical salts, **37** has an HCP anion with charge of −2, judging from the CN stretching frequencies (2185, 2165 cm^{-1}), which are in good agreement with the reported values for HCP^{2-} (2183−2184, 2165−2168 cm^{-1}).[34] This is also confirmed by a skeletal vibrational band observed in the frequency region expected for the dianion (∼1400 cm^{-1}) rather than for the monoanion (∼1490 cm^{-1}). The charges on other anions are assigned as −2 in **31** and **32**, and −1 in **33**, **35**, and **36**, because these anions have too high potentials (≥0.96 V vs SCE, Table 4) to be oxidized by a BEDO-TTF$^+$ molecule ($E_{1/2}^1$(D) = 0.43 V). The γ values are 0.40 for **31**, **33**, and **37**, and 0.50 for **32**, **35**, and **36**, respectively, simply on the basis of the stoichiometry. Since the charge on SQA is generally −2, and since SQA^- is detected only in solution,[35] the γ of **34** is expected to be 0.5 on the basis of the ratio BEDO-TTF/SQA = 4.

It becomes rather complicated to estimate γ values for other complexes in Table 5 (**6**−**25**). Hence, we tried more quantitative analysis of the ionicity of the complexes based on vibration frequencies of the BEDO-TTF molecules. Moldenhauer et al. have reported that the four absorption bands of BEDO-TTF^0 [864 (band a), 963 (b), 1011 (c), and 1082 cm^{-1} (d)] display ionization frequency shifts on the CT complex formation.[36] The vibrational bands of **31** in the region 800−1200 cm^{-1} (Figure 4a) are derived solely from those observed in BEDO-TTF^0; three prominent bands at 861 (a), 1006 (c), and 1179 cm^{-1} (e) and two weaker bands at 957 (b) and 1080 cm^{-1} (d). The band e is ascribed to that of BEDO-TTF^0 at 1159 cm^{-1}. Very similarly spectra are observed for all other metallic BEDO-TTF complexes and for highly conducting semiconductors **13** and **37**.

According to the normal coordinate analysis for neutral BEDO-TTF, the above five bands involve vibrations of C−O bonds.[37] Bands a, d, and e include the vibration between the terminal ethylene carbon and the oxygen atom. Therefore, these vibrations may be affected not only by the electronic structure, but also by the structural interactions with the counter components in the vicinity of the terminal ethylene groups. Band b shows an intensity too weak for determination of accurate frequencies for some BEDO-TTF complexes. On the other hand, the intense band c ($b_{1u}\nu_{31}$ mode), which is dominated by C_{in}−O and C_{in}−S stretches (C_{in}; the carbon atoms of the vinyl

(34) LePage, T. J.; Breslow, R. *J. Am. Chem. Soc.* **1987**, *109*, 6412.
(35) Patton, E. V.; West, R. *J. Phys. Chem.* **1973**, *77*, 2652.
(36) Moldenhauer, J.; Pokhodnia, K. I.; Schweitzer, D.; Heinen, I.; Keller, H. J. *Synth. Met.* **1993**, *55*−*57*, 2548.
(37) Pokhodnia, K. I.; Kozlov, M. E.; Onischenko, V. G.; Schweitzer, D.; Moldenhauer, J.; Zamboni, R. *Synth. Met.* **1993**, *55*−*57*, 2364.

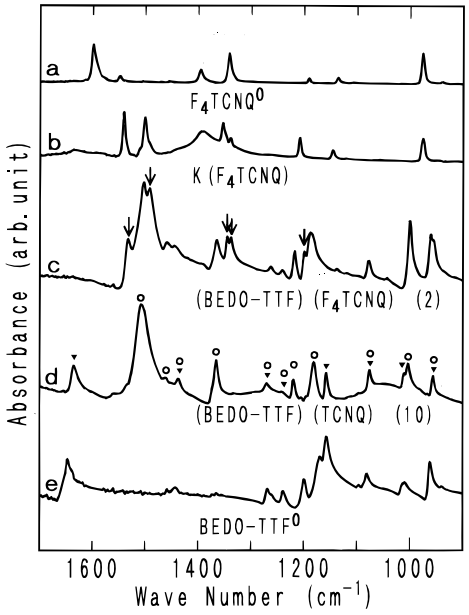

Figure 3. IR spectra of (a) neutral F_4TCNQ, (b) $K(F_4TCNQ)$, (c) (BEDO-TTF)(F_4TCNQ) (**2**), (d) (BEDO-TTF)(TCNQ) (**10**), and (e) neutral BEDO-TTF on KBr pellet. The vibrational bands of F_4TCNQ^- are represented by arrows for complex **2**. The vibrational bands designated by open circles and filled triangles are ascribed to those of ionized and neutral BEDO-TTF molecules, respectively.

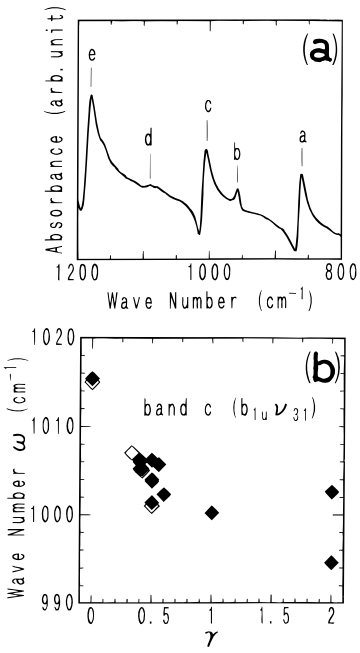

Figure 4. (a) IR spectra of (BEDO-TTF)$_5$(HCTMM)(PhCN)$_2$ (**31**) in the KBr disk. See text for the assignment of a−e. (b) Dependence of the frequency (ω) of $b_{1u}\nu_{31}$ mode on the average charge on the donor, γ. The results of this work are represented by filled squares for neutral BEDO-TTF and its CT complexes of known γ (**1**−**5**, **31**−**37**, (BEDO-TTF)I_3)$_2$ ($\gamma = 2$),[39] (BEDO-TTF)I_{10-y} ($\gamma = 2$)[39]). Open squares represent the reported data for neutral BEDO-TTF[37] and its radical salts[36] with $Cu_2(NCS)_3^-$ ($\gamma = 0.33$), I_3^- (0.42), and ReO_4^- (0.50).

ether), is expected to be relatively insensitive to structural interactions with counter components. Consequently, we have examined whether this vibrational frequency (ω) is useful for estimating γ of the complexes.

Figure 4b plots the ω values obtained from the measurements with higher resolution (0.5 cm^{-1}) against the γ for neutral BEDO-TTF[37,38] and its complexes of unambiguously known γ (**1**−**4**, **31**−**33**, and **35**−**37**), as well as the reported γ values.[36] Also plotted are the data for dication salts (BEDO-TTF)$(I_3)_2$ and (BEDO-TTF)I_{10-y} ($y = 0.4-0.5$), the details of which are reported elsewhere.[39] Although the band c tends to show red shift upon ionization, the correlation is not good enough for the accurate estimation of unknown γ of the complexes; the ω values are scattered by 5 cm^{-1} at $\gamma = 0.5$ and by 8 cm^{-1} at $\gamma = 2$.

Even with fully ionic acceptor molecules, partial γ values are deduced for all the metallic BEDO-TTF complexes containing excess donor molecules. On the basis of the stoichiometry, γ values of **12** and **20** are at most 0.40 and 0.46, respectively. The superconducting $(BEDO\text{-}TTF)_3Cu_2(NCS)_3$ has an even further lowered γ (0.33).[15a] It has been previously established that in most DA-type complexes of $\gamma < 0.5$, the alternating stack is stable rather than the segregated one, resulting in an insulating ground state. As far as we know, metals which feature both uniformly segregated stacks and low γ (<0.5) have been obtained only from molecules much larger than BEDO-TTF, as exemplified by $(DTEDT)_3Au(CN)_2$ ($\gamma = 0.33$) and nickel phthalocyanine triiodide ($\gamma = 0.33$).[40]

For the insulating **26**−**30**, each IR spectrum is approximated by the superposition of the spectra of the neutral components, confirming that they are neutral complexes.

The electronic state is somewhat complicated in the semiconducting (BEDO-TTF)(TCNQ) (**10**). The IR spectrum shows three CN stretching bands around 2210−2150 cm^{-1}. The highest frequency band ($b_{1u}\nu_{19}$ mode), which is often used to determine the charge on the TCNQ molecules (ζ) in its CT complexes,[29] is observed at 2194 cm^{-1} with a shoulder at 2201 cm^{-1}. Their frequency shifts ($\Delta\omega$) from neutral TCNQ (2225 cm^{-1}) suggest the fractional charge ($\zeta = 0.55-0.70$), using the proposed formula $\Delta\omega/\zeta = 44$ cm^{-1}.[29] Such a splitting of $b_{1u}\nu_{19}$ mode is observed, not in the metallic temperature region of TTF-TCNQ, but below 55 K, where CDW drives the distortion on TCNQ stacks.[41] The crystal structure of **10**, although unknown at present, likely contains distorted TCNQ stacks. Through comparison with the spectra of $(BEDO\text{-}TTF^+)(F_4TCNQ^-)$ (**2**) (Figure 3c) and $TCNQ^n$ ($n = 0, -1$),[42] most of the vibrational bands of **10** can be assigned to those of $BEDO\text{-}TTF^+$ (designated by open circles in Figure 3d) and $TCNQ^{-\zeta}$. There remain three unassigned bands at 1010, 1159, and 1635 cm^{-1}, which are in turn ascribable to those of neutral BEDO-TTF (filled triangles in Figure 3d are those ascribable to neutral BEDO-TTF (Figure 3e)). These facts suggest a charge separation among BEDO-TTF molecules.[43] Partially charged TCNQ

(38) The neutral BEDO-TTF shows two bands at 1011 and 1015 cm^{-1}. The former is assigned to the totally symmetric ($a_g\nu_7$) mode,[37] which becomes infrared active due to the deformed molecular structure (tub-shape) from the D_{2h} symmetry. The authors in ref 36 show the frequency shifts based from 1011 cm^{-1}. However, this a_g mode should be infrared inactive in the CT complexes, where the flat donor molecules with almost D_{2h} symmetry tend to stack regularly (see later text). Even the ReO_4 salt, where slightly dimerized donor molecules construct the layers, shows no corresponding vibronic bands around 1000 cm^{-1} in the reflectance spectra along the donor layer. Swietlik, R.; Kushch, N. D. *Phys. Stat. Sol.* (*a*) **1994**, *142*, 515. Thus we utilize the normal active $b_{1u}\nu_{31}$ mode at 1015 cm^{-1} in Figure 4b.

(39) Horiuchi, S.; Yamochi, H.; Saito, G.; Matsumoto, K. *Mol. Cryst. Liq. Cryst.* **1996**, *284*, 357.

(40) (a) Misaki, Y.; Higuchi, N.; Fujiwara, H.; Yamabe, T.; Mori, T.; Mori, H.; Tanaka, S. *Angew. Chem.* **1995**, *34*, 1222. T. Mori corrected the stoichiometry of DTEDT-$Au(CN)_2$ salt in "Workshop on Molecular Superconductors" in Kyoto, Japan (Nov 16−18, 1995). (b) Schramm, C. J.; Scaringe, R. P.; Stojakovic, D. R.; Hoffman, B. M.; Ibers, J. A.; Marks, T. J. *J. Am. Chem. Soc.* **1980**, *102*, 6702.

(41) Etemad, S. *Phys. Rev. B* **1981**, *24*, 4959.

(42) Bozio, R.; Zanon, I.; Girlando, A.; Pecile, C. *J. Chem. Soc., Faraday Trans. 2* **1978**, *74*, 235.

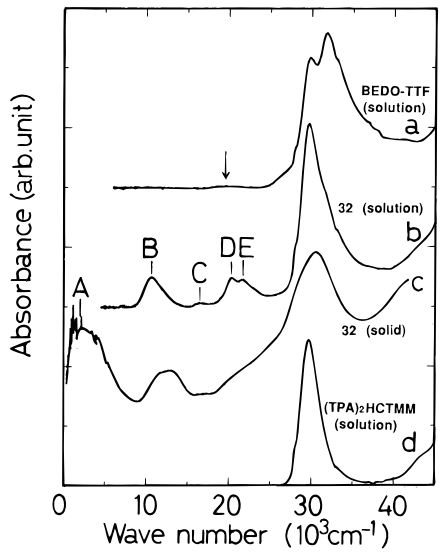

Figure 5. Optical absorption spectra of (a) neutral BEDO-TTF in AN solution, (b) $(BEDO\text{-}TTF)_4(HCTMM)(TCE)_2$ (**32**) in AN solution, (c) **32** on KBr pellet, and (d) $(TPA)_2HCTMM$ in AN solution. The arrow indicates the absorption at 19.5×10^3 cm^{-1}. See text for assignment of A−E.

stacks are therefore considered to afford relatively high conductivity to **10** although their distortion seems to prevent metallic conduction.

In summary, the CT complexes with neutral (**26**−**30**), fully ionic (**2**), or inhomogeneous charge-distributed ground states (**10**) resulted in semiconducting electronic properties, whereas all the others, which were in the partial CT ground state of the donor, resulted in metals, with the exception of only two complexes with $C_{14}TCNQ$ (**13**) and HCP (**37**). It should be emphasized that BEDO-TTF has peculiar ability to afford metals of small γ among the TTF-based donors.

Electronic Spectrum. Neutral BEDO-TTF in solution exhibits strong absorption bands at 29.9×10^3 and 31.8×10^3 cm^{-1} and much weaker one at 19.5×10^3 cm^{-1} (Figure 5). These bands also appear at almost the same energy in the solid state, but the lowest one (19.9×10^3 cm^{-1}) increases in relative intensity. In addition, the higher energy bands [$(25-35) \times 10^3$ cm^{-1}] are poorly resolved compared to the solution spectrum. These features correspond well with those observed for BEDT-TTF.[44]

Table 5 summarizes the energies of the lowest transitions ascribable to CT ($h\nu_{CT}$) and high-energy transitions (UV−vis) for all the BEDO-TTF complexes. First, we describe the absorption spectra of $(BEDO\text{-}TTF)_4(HCTMM)(TCE)_2$ (**32**) as a typical example of the metals. The solution spectrum (Figure 5b) reveals an intense band at 29.7×10^3 cm^{-1}, hiding the bands of neutral BEDO-TTF. Comparison with the spectrum of $(TPA)_2HCTMM$ (Figure 5d) allows us to assign this band to the intramolecular excitation of $HCTMM^{2-}$. Other bands appear at 10.7×10^3, 16.7×10^3, 20.4×10^3, and 21.6×10^3 cm^{-1}, labeled as B, C, D, and E, respectively, in Figure 5b.

The powder spectrum of **32** (Figure 5c) shows an additional band (band A) around 2.3×10^3 cm^{-1}. This low-lying absorption arises from the CT transition: $(BEDO\text{-}TTF)^0 + (BEDO\text{-}TTF)^+ \rightarrow (BEDO\text{-}TTF)^+ + (BEDO\text{-}TTF)^0$. The powder spectra of all other metals and of highly conducting **10**, **13**, and **37** also show the A band extending throughout the whole infrared region. With few exceptions,[45] the appearance of the A band ($\leq 5 \times 10^3$ cm^{-1}) indicates both the partial CT state and segregated or self-assembling state of the component molecule[5b] that are essential for the metallic conduction.

The peak B in the solid spectrum is broadened and shows a blue shift of about 2×10^3 cm^{-1} vs that in solution. The B band is observable in the powder spectra of all the metallic BEDO-TTF complexes (Table 5). In the solution spectra of TTF^+, while the lowest transition is situated at 17×10^3 cm^{-1} for the monomer,[46] its dimer gives rise to an additional band at the lowered energy (14×10^3 cm^{-1}),[47] which corresponds to the CT process, $(TTF)^+ + (TTF)^+ \rightarrow (TTF)^0 + (TTF)^{2+}$. The latter transition energy is related to the effective on-site Coulomb repulsion (U_{eff}) on TTF. In the present case, however, the band B can be related to the lowest intramolecular excitation rather than this CT process for the following reasons: (i) The band B is clearly observed even for complexes of small γ (for example, 0.5 for **32**). This contradicts what has been theoretically[48] and experimentally[46,49] observed for the CT process among TTF^+ radicals; intensity of band B is greatly diminished with decrease of γ and vanishes where $\gamma = 0.5$. (ii) On the other hand, for the fully ionic $(BEDO\text{-}TTF)I_3$ salt,[39] which contains $(BEDO\text{-}TTF^+)_2$ dimers in its crystals, the solid spectrum reveals low-energy bands [$(7-9) \times 10^3$ cm^{-1}] in addition to band B; hence these new bands are assigned to the CT between $BEDO\text{-}TTF^+$ molecules. This CT transition energy is considerably small in comparison to TTF (14×10^3 cm^{-1}), indicating the reduction of U_{eff} for the BEDO-TTF molecule. (iii) The equilibrium between cation monomer and its dimer in solution gives rise to a concentration dependence of the absorbance. However, the absorbance of band B of **32** ($\epsilon = 4.0 \times 10^3$ per mole of $BEDO\text{-}TTF^+$) is independent of the concentration of $BEDO\text{-}TTF^+$ (1×10^{-6} to 4×10^{-5} mol L^{-1}). (iv) BEDT-TTF radical salts reveal their absorption band at about 10×10^3 cm^{-1} in the spectra polarized along the long axis of the donor molecule; this spectrum is assigned to their lowest intramolecular excitation.[50] This transition was explained by an electronic one from the second highest occupied molecular orbital (SHOMO) to the HOMO, which accommodates an unpaired electron in the ground state.[46] According to the PES measurement,[22] the differences between the first and second ionization potentials for BEDO-TTF (1.01 eV) and BEDT-TTF (∼1.2 eV) are much smaller than that for TTF (1.88 eV). The decrease of the energy difference between HOMO and SHOMO for BEDO-TTF is in good agreement with the magnitude of the red shift of the band B (17×10^3 cm^{-1} (TTF^+) → 10.7×10^3 cm^{-1} ($BEDO\text{-}TTF^+$), decrease by 0.8 eV). On the basis of the items i−iv, the band B in solution can be assigned to the lowest intramolecular excitation. B band in the solid is also assignable to this transition. However, because the BEDO-TTF molecules are not strictly perpendicular to the stack in the crystal, the CT

(43) The complex **10** is regarded as a single phase because the appearances and the IR spectra are unchanged under the different preparation conditions.

(44) Kozlov, M. E.; Tanaka, Y.; Tokumoto, M.; Tani, T. *Chem. Phys. Lett.* **1994**, *223*, 318.

(45) A band below 5×10^3 cm^{-1} appears in a system of a Mott insulator of an extremely small on-site Coulomb repulsion (example, $(BDNT)PF_6$, BDNT = 4,9-bis(1,3-mercaptobenzo-2-ylidene)-4,9-dihydronaphtho[2,3-*c*]-[1,2,5]thiadiazole): Dong, J.; Yakushi, K.; Yamashita, Y. *J. Mater. Chem.* **1995**, *5*, 1735.

(46) Sugano, T.; Yakushi, K.; Kuroda, H. *Bull. Chem. Soc. Jpn.* **1978**, *51*, 1041.

(47) Torrance, J. B.; Scott, B. A.; Welber, B.; Kaufman, F. B.; Seiden, P. E. *Phys. Rev. B* **1979**, *19*, 730.

(48) Maldague, P. F. *Phys. Rev. B* **1977**, *16*, 2437.

(49) Jacobsen, C. S.; Tanner, D. B.; Bechgaard, K. *Phys. Rev. B* **1983**, *28*, 7019.

(50) Sugano, T.; Hayashi, H.; Kinoshita, M.; Nishikida, K. *Phys. Rev. B* **1989**, *39*, 11387.

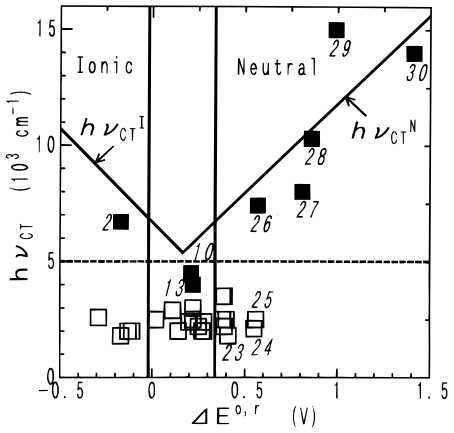

Figure 6. Comparison of CT bands of BEDO-TTF complexes of DA-type on KBr pellet ($h\nu_{CT}$) and $\Delta E^{o,r}$ ($= E_{1/2}{}^{1}(D) - E_{1/2}{}^{1}(A)$). Semiconducting and metallic complexes are represented by filled and open squares, respectively. For assignment of the V-shaped, vertical, and horizontal dotted lines, see text. Numbers represent the entry numbers of the complexes.

processes creating the doubly occupied states may be mixed in this band, as has previously been proposed for β-(BEDT-TTF)$_2$I$_3$.[51]

By analogy with TTF salts,[46,47] bands C, D, and E observed in the solution of **32** are attributable to the intramolecular transition of BEDO-TTF$^+$. In the powder spectrum, these bands are broadened, poorly resolved, and in some cases, observed only as shoulders due to a solid-state effect. The metallic BEDO-TTF complexes of DA-type yield further complicated solid spectra due to the superimposed absorptions of ionized acceptors.

The CT band of the alternating stacking type is related to the transition from $D^{+\gamma}A^{-\gamma}$ to $D^{+(1-\gamma)}A^{-(1-\gamma)}$. This band's transition energies for neutral ($h\nu_{CT}{}^{N}$) and ionic complexes ($h\nu_{CT}{}^{I}$) are represented differently[24,52] as

$$h\nu_{CT}{}^{N} = I_P(D) - E_A(A) - C' + X \quad (\gamma < 0.5) \quad (4)$$

$$h\nu_{CT}{}^{I} = -I_P(D) + E_A(A) + (2\alpha - 1)C' + X' \quad (\gamma > 0.5) \quad (5)$$

Here α is the Madelung constant, C' is the averaged electrostatic attraction energy of a D−A pair (defined as positive), and X, X' are mainly the resonance stabilization energies. Since the $E_A(A)$ data are not available for all the acceptors used, the $\Delta E^{o,r}$ ($= E_{1/2}{}^{1}(D) - E_{1/2}{}^{1}(A)$) value, which is originally related to the adiabatic values, $I_P{}^{ad}(D)$ and $E_A{}^{ad}(A)$ as previously described, is often used instead of the $I_P(D) - E_A(A)$.

Figure 6 shows a plot of $h\nu_{CT}$ vs $\Delta E^{o,r}$ for all the BEDO-TTF complexes of DA-type. Equations 4 and 5 are portrayed in the figure as a V-shaped line (Torrance's diagram).[52] This diagram helps us to predict the stacking manner and ionicity of a CT complex[52,53] with some care.[54] The open and filled squares in the figure represent metallic and semiconducting complexes, respectively. The neutral BEDO-TTF complexes, **26**, **28**, and **30** locate along the V-shape line, which corresponds to the CT transition from donor to acceptor molecule. The CT transitions in **27** and **29** can also be related to the same type in consideration of their crystal structures (see below). The irreversible reduction processes of these acceptor molecules prevent the accurate determination of $\Delta E^{o,r}$ values, which may be responsible for the deviation from the V-shaped line.

On the other hand, the metallic complexes and highly conducting semiconductors **10** and **13** yield CT bands (band A) at much lower energy ($\leq 5 \times 10^3$ cm^{-1}, below the dotted line in Figure 6). In the case of (BEDO-TTF)(TCNQ) (**10**), our previous discussion of the IR spectrum suggests both the charge separation among BEDO-TTF molecules and the partial CT ground state of TCNQ molecules. Therefore, the TCNQ stack is likely to dominate the conductivity and contribute to the A band (4.5×10^3 cm^{-1}).

The overall spectrum of the fully ionic (BEDO-TTF)(F$_4$-TCNQ) (**2**) is complicated and similar to that for (BEDT-TTF)-(F$_4$TCNQ) of mixed stacking type;[12b,j] the absorption bands appear at 6.7×10^3, 9.3×10^3, 12×10^3, 13×10^3, and 26×10^3 cm^{-1} for the former complex, and at 6.1×10^3, 9.3×10^3, 14×10^3, and 26×10^3 cm^{-1} for the latter. The high CT transition energy of **2** (6.7×10^3 cm^{-1}) corresponds to the insulating nature. Considering that this energy is also close to the CT transition energy among F$_4$TCNQ$^-$ molecules (6.3×10^3 cm^{-1} for K(F$_4$TCNQ)), it is currently difficult to predict stacking type in **2**.

The above results consistently indicate that the lowest absorption band of each BEDO-TTF complex is ascribable to that CT process with transition energy correlated to the conducting property.

Features of Acceptors in Metallic Complexes. One of the peculiar features of the BEDO-TTF complexes is that the metals are fertile with regard to shape and size of the acceptor molecules. Ten metals are obtained from acceptors with the TCNQ skeleton, one of the traditional superior building blocks of organic metals. Even THBTCNQ and DHBTCNQ possessing bulky substituents which tend to prohibit uniform stacking, provided good metals ($\sigma_{rt} = 110$ and 33 S cm^{-1}, respectively) of very low $T_{\sigma_{max}}$. Although the bulky substituents without delocalized π-electrons in their acceptors are regarded as disadvantageous for the highly conducting metals, BEDO-TTF can yield a metal **12**, and a highly conducting complex **13**. It is noteworthy that we have found also the metallic nature of **12** and **18** on the LB films.[55] Metallic complexes are also derived from nine out of ten *p*-benzoquinone derivatives, which have been known to form alternating stack, preferably in CT complexes. The percyanoolefins (HCBD and TCNE) are no exception, despite the fact their component molecules are inferior for producing usual organic metals. Furthermore, this donor allows metals with two fluorene derivatives for the first time. These facts indicate that BEDO-TTF molecules construct the metallic columns or layers preferably and that counter molecules serve the functions of charge compensating and/or space filling.

Another interesting feature is the strength of acceptor molecules for producing metallic BEDO-TTF complexes. In the 1:1 TTF-TCNQ system the following condition is required for organic metals: $-0.02 \leq \Delta E^{o,r} \leq 0.34$ V,[6] the boundaries of which are shown by vertical lines in Figure 6. BEDO-TTF ($E_{1/2}{}^{1}(D) = +0.43$ V) meets this criterion for 12 acceptors used, 10 of which actually gave metals.

(51) Jacobsen, C. S.; Tanner, D. B.; Williams, J. M.; Geiser, U.; Wang, H. H. *Phys. Rev. B* **1987**, *35*, 9605.

(52) Torrance, J. B.; Vazquez, J. E.; Mayerle, J. J.; Lee, V. Y. *Phys. Rev. Lett.* **1981**, *46*, 253.

(53) Nakasuji, K. *Pure Appl. Chem.* **1990**, *62*, 477.

(54) Some fully ionic complexes with alternating stacking show the absorptions of CT progress among D^+ (or A^-) molecules instead of the back CT absorption (from A^- to D^+) (e.g. (BEDT-TTF)(F$_4$TCNQ)[12j]). Therefore, strictly speaking, the stacking types are not determined solely from the analysis of Torrance's diagram, although such exceptions are few.

(55) (a) Nakamura, T.; Yunome, G.; Azumi, R.; Tanaka, M.; Tachibana, H.; Matsumoto, M.; Horiuchi, S.; Yamochi, H.; Saito, G. *J. Chem. Phys.* **1994**, *98*, 1882. (b) Ogasawara, K.; Ishiguro, T.; Horiuchi, S.; Yamochi, H.; Saito, G. *Jpn. J. Appl. Phys.* **1996**, *35*, L571.

In general, 1:1 CT complexes are fully ionic insulators in the region $\Delta E^{o,r} < -0.02$ V, and (BEDO-TTF)(F_4TCNQ) (**2**) is just such a case ($\Delta E^{o,r} = -0.17$ V). Although other acceptors in the same region (for **1**, **3**−**5**) are also fully ionized, non 1:1 stoichiometries will allow partial oxidation of the donor and resultant metallic state.

Segregated stacking is rarely found in complexes beyond the other boundary of $\Delta E^{o,r} = 0.34$ V, which has been regarded as corresponding to $\gamma = 0.5$. Nevertheless, this region involves eight metallic BEDO-TTF complexes. The $\Delta E^{o,r}$ values of **24** and **25** are highest among these, but still somewhat uncertain due to the irreversible reduction of acceptors. At present it seems evident that the upper boundary of $\Delta E^{o,r}$ for metallic BEDO-TTF complexes locates between +0.41 V (**23**) and +0.57 V (**26**), considerably higher than conventional TTF-TCNQ-based organic metals.

The above results lead to the conclusion that BEDO-TTF molecules can construct the self-aggregated (segregated columnar or layered) structure so easily that the acceptor molecules of a wide variety of shapes, sizes, and strengths are allowed to yield organic metals. The following structural properties will clarify the origin of this strong self-aggregating ability.

Crystal Structures of $(BEDO\text{-}TTF)_5(HCTMM)(PhCN)_2$ (31) and $(BEDO\text{-}TTF)_{10}(CF)_4(H_2O)_3$ (33). These two salts show common structural features, which are discussed together here. The triclinic unit cells (Table 3) contain five and one donor molecules for **31** and **33**, respectively. As distinct from the tub shape in the neutral crystal,[13a] BEDO-TTF molecules are almost planar, except for the terminal ethylene groups of the eclipsed conformation. This molecular structure can be commonly seen in most of the BEDO-TTF salts. The rigidity of the ethylene groups makes a striking contrast with the BEDT-TTF salts, in which various conformations are allowed and in some cases are related to the salt's physical properties.[56]

The donor molecules form layers along the *ac* planes (Figure 7a), where they stack along the $a + 2c$ and c directions for **31** and **33**, respectively. Their layered arrangements are similar to those of $(BEDO\text{-}TTF)_{2.4}I_3$ salt,[14a] and will be designated as the I_3 type donor packing in this paper.

To compare the stacking manner of the BEDO-TTF salts, we defined the three structural parameters, D, δ, and ϵ (Figure 7b and 7c). D is the intermolecular separation along the stack obtained by averaging the atomic displacement of the $C_6O_4S_4$ moiety (excluding the ethylene groups) from the neighboring molecular plane. δ and ϵ are the tilted (acute) angles of the stacking direction with the molecular plane and with the central C═C bond, respectively (Table 6). The stacking axis in **33** tilts by 60.6° to the molecular plane with D of 3.51 Å and ϵ is 90.0°, indicating slipped stacking only along their transverse directions. In the case of **31**, little variation in the crystallographically independent D (3.48−3.59 Å), δ (59.0−62.3°), and ϵ (87.5−89.5°) indicates the almost uniform stacking. Furthermore, these values are very close to those of **33**.

The donor molecules in **31** and **33** show short intermolecular C−H···O contacts (H···O distance < 2.72 Å, dotted lines in Figure 7b for **31**), although no S···S and S···O contacts shorter than the van der Waals radii (vdW) sums exist along the stack.[57]

Each donor molecule is linked by three S···S (3.40−3.49 Å) and two S···O (3.27−3.28 Å) short atomic contacts with coplanar neighboring ones (side-by-side contact) along the $3a + c$ and $a + c$ directions in **31** and **33**, respectively (See Figure 7d for **31**).

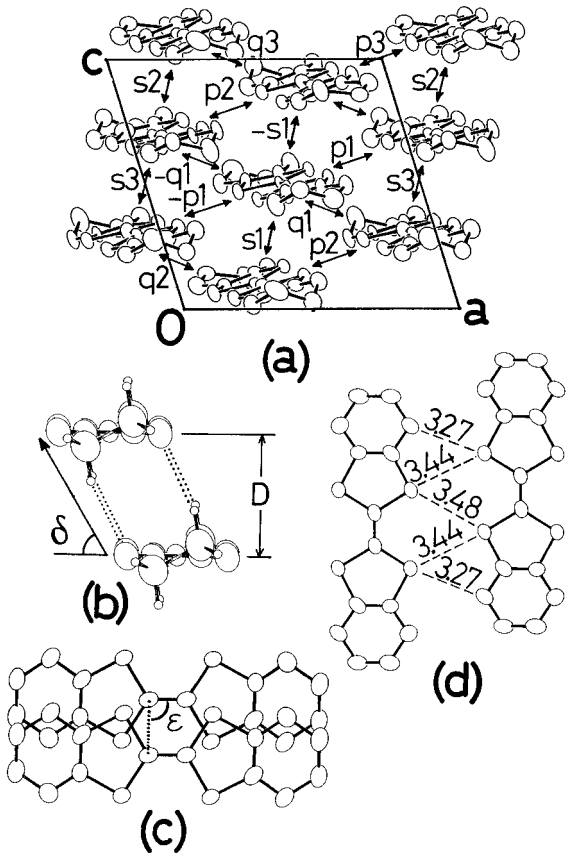

Figure 7. Crystal structures of $(BEDO\text{-}TTF)_5(HCTMM)(PhCN)_2$ (**31**): (a) the molecular arrangement in a donor layer viewed along the *b* axis with scheme of the intermolecular overlap integrals; (b) stacking motif of the donor molecules projected along the long direction of the molecule; intermolecular short C−H···O contacts (H···O < 2.72 Å) are shown by dotted lines; (c) stacking motif of the donor molecule viewed on the molecule; (d) side-by-side arrangement of the donor molecules. The averaged distances are shown in angstroms. Hydrogen atoms are omitted for clarity in the a, c, and d. For s_i, p_i, q_i ($i = 1-3$), D, δ, and ϵ, see text.

In neither salt could we determine the position of the counter components due to the components' severe disorder. This may indicate that the periodicities of the counter molecules are disregarded during formation of the uniform donor array.

Crystal Structure of $(BEDO\text{-}TTF)_4(SQA)(H_2O)_6$ (34). The parameters c and V of the triclinic cell are twice the corresponding values for **33** (Table 3). The BEDO-TTF molecules locate on two nonequivalent inversion centers and reveal the same molecular structure as those in **31** and **33**. The planar squarate and a pair of water molecules occupy the corner of the unit cell with the respective weight of $^1/_2$.

The donor molecules form a layer along the *ac* plane (Figure 8a) with c as the stacking axis. The donor packing shares most of the features of that in **31** and **33** (the I_3 type).

However, the interstack array is slightly modified; the molecules adjacent along the $a - 2c$ direction are nearly coplanar (dihedral angle of 4.6°) but the numbers of short atomic contacts is decreased; two S···S (3.39−3.54 Å) and one S···O (3.09 Å) distances are shorter than the vdW sums.

The squarate molecules are packed parallel to the *ac* plane, forming a sheet with water molecules (Figure 8). The oxygen atoms construct a 2D network of the intermolecular hydrogen bonds (O···O distance ∼2.8 Å; dotted lines in Figure 8b).

(56) Leung, P. C.; Emge, T. J.; Beno, M. A.; Wang, H. H.; Williams, J. M.; Petricek, V.; Coppens, P. *J. Am. Chem. Soc.* **1985**, *107*, 6184.

(57) The van der Waals radii (vdW) employed in this paper are as follows; C 1.70 Å, H 1.20 Å, N 1.55 Å, O 1.52 Å, S 1.80 Å. Bondi, A. *J. Phys. Chem.* **1964**, *68*, 441.

Table 6. Comparison of the Packing Motifs of the Donor Molecules and the Results of Band Calculation of BEDO-TTF Radical Salts

	counter anion									
	I_3^-	CF^-(**33**)	$HCTMM^{2-}$(**31**)	SQA^{2-}(**34**)	ClO_4^-	$AuBr_2^-$	$Cu_2(NCS)_3^-$	ReO_4^-	HCP^{2-}(**37**)	Cl^-
donor packing type	I_3	I_3	I_3	I_3	I_3	I_3	I_3	I_3	HCP	Cl
D, Å[a]	3.50	3.51	3.48−3.59	3.54−3.58	3.50	3.45−3.59	3.60−3.67	3.44−3.49	3.52	3.54
δ, deg[a]	60.4	60.6	59.0−62.3	59.8−60.8	60.3	57.7−61.4	56.4−59.4	58.7−59.4	59.4	43.8
ϵ, deg[a]	89.2	90.0	87.5−89.5	86.6−88.5	89.5	88.9−89.0	88.3−88.9	88.1−89.9	88.6	87.3
no. of C−H··O contacts (H··O 2.72 Å) per one donor molecule										
intrastack	4.0	4.0	3.2	2.0	4.0	2.0	1.3	3.0	3.0	0.0
interstack	0.0	0.0	0.4	0.0	0.0	1.0	0.7	0.5	0.0	2.0
interaction type [overlap integral ($\times 10^3$)]										
intrastack										
s1	5.5	5.9	−5.6	5.3	5.9	−5.2	5.3	3.3	5.6	
s2			3.8	6.2			−4.3	4.8		
s3			−3.7							
r										−11.4
interstack										
p1	15.2	14.9	−12.9	12.3	14.1	−14.6	−13.2	11.7	−13.8	
p2			−13.2				−10.2	12.8		
p3			−14.6							
q1	−13.0	−13.3	−15.6	−13.5	−13.6	−9.3	−10.0	−13.3	13.3	
q2			14.4			−14.4	12.6	−14.7		
q3			9.8							
u									−7.8	
w										−14.6
$N(E_F)$[b]	1.30	1.26	1.36	1.46	1.40	1.30	1.46	1.46	1.93	1.20
band width, eV	1.13	1.13	1.10	1.03	1.11	1.07	0.92	1.05	0.73	1.22
S_{FS}/S_{BZ}, % (center)	42(Y)	40(Z)	25(B)	8.0(X) 2.8(B) 5.1(Z)	1.7(Z)	−	50(X)	8.4(X) 6.5(B) 2.0(Z)		50(Γ)
ref[c]	14a				14c	14c	15a	14e		14e

[a] See text for the definitions of *D*, δ, ϵ, and S_{FS}/S_{BZ} and the labeling of the intermolecular interactions. [b] Fermi-level DOS; units, states(total)/(eV molecule of BEDO-TTF). [c] The packing parameters were obtained based on the crystal structures in the references.

The interactions between donor and counter components are dominated by a number of C—H···O contacts (H···O distance <2.72 Å), which are the likely origin of the slightly modified interstack array of the donor.

Crystal Structure of $(BEDO\text{-}TTF)_5(HCP)(PhCN)_{0.2}$ (37). The monoclinic unit cell with the parameters shown in Table 3 contains one crystallographically independent BEDO-TTF molecule, the structure of which is the same as in **31** and **33**. The donor packing in the accurate cell (*a*, 5*b*, *c*) must be unchanged from this averaged one because the thermal parameters are normal for any atoms of the donor molecule. This is also supported by the fact that the superlattice gives few and weak reflections.

The anion molecules alternate with donor layers (the *bc* plane). The donor molecules stack along the *b* axis (Figure 9). The donor packing is somewhat different from that of other BEDO-TTF salts, so it will be designated as HCP type. Each donor layer consists of a repetition of four stacks (Figure 9a). The stacks A (or B) and A′ (or B′) are related to each other by the inversion centers; hence, the molecular planes are parallel. On the other hand, the stack B′ is related to the stack A by the 2-fold screw axis ($x = {}^1/_2$, $z = {}^1/_4$) with the dihedral angle of 60.2°. Consequently, the molecular planes alternate every two stacks to form an AA′BB′ stack array. Such a packing motif resembles that in α″-$(BEDT\text{-}TTF)_2CsHg(SCN)_4$.[58]

Donor packing in the stack pairs AA′ or BB′ shows the same pattern as the I_3 type, as is evident from both the similar values of *D*, δ, and ϵ and the existence of the intermolecular short C—H···O contacts. The molecules A1 and A′1 in Figure 9a are coplanarly linked side-by-side with each other by three S···S (3.41−3.51 Å) and two S···O (3.26 Å) short atomic contacts like those of **31** and **33**.

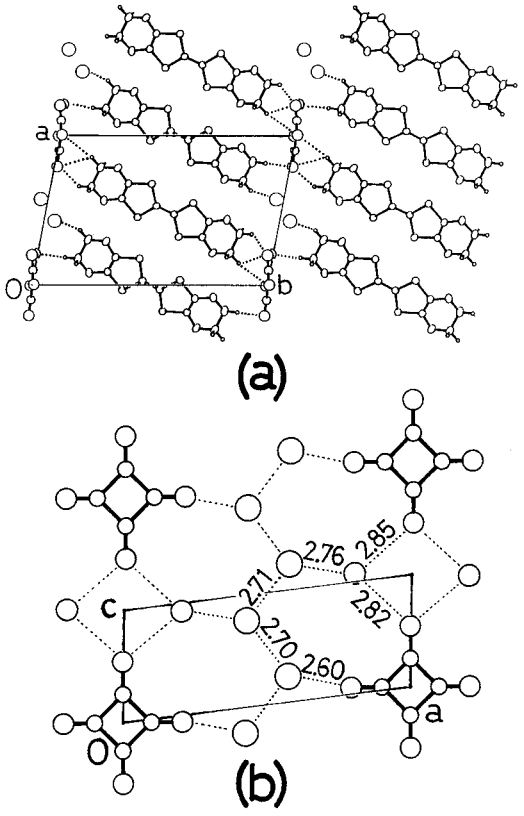

Figure 8. Crystal structures of $(BEDO\text{-}TTF)_4(SQA)(H_2O)_6$ (**34**): (a) crystal structure projected on the *c* axis; intermolecular short C—H···O contacts (H···O < 2.72 Å) between the donor and counter component molecules are shown by dotted lines; and (b) arrangement of the squarate ions and water molecules; intermolecular hydrogen bonds (OH···O, Å) are shown by dotted lines (hydrogen atoms are not depicted).

(58) Mori, H.; Tanaka, S.; Mori, T.; Maruyama, Y.; Inokuchi, H.; Saito, G. *Solid State Commun.* **1991**, *78*, 49.

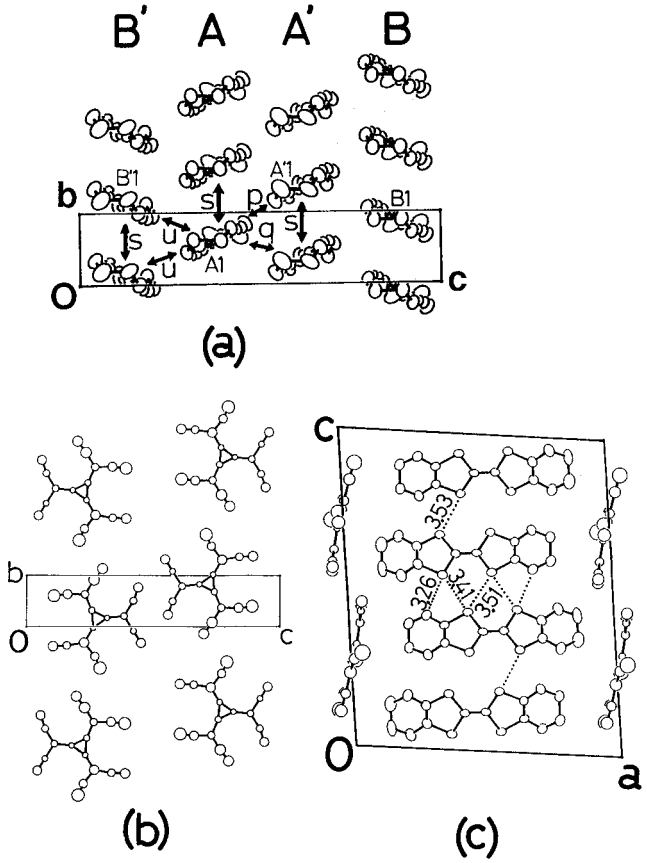

Figure 9. Crystal structures of $(BEDO\text{-}TTF)_5(HCP)(PhCN)_{0.2}$ (**37**): (a) layer of BEDO-TTF molecules viewed along the *a* axis with scheme of the intermolecular overlap integrals (*s*, *p*, *q*, *u*); with regard to A, A′, B, B′, A1, A′1, and B1, B′1, see text; (b) arrangement of HCP^{2-} molecules viewed along the *a* axis; (c) crystal structure viewed along the *b* axis. The dotted lines show atomic S···S and S···O contacts among the molecules A1, A′1, B1 and B′1 with the distances (Å).

However, the molecules A1 and B′1, which are inclined to each other, have only one short S···S contact (3.53 Å) (Figure 9c).

The planar HCP anions, the molecular planes of which tilt by 76° to the long axis of the donor molecule, form the periodicity of 5*b* (Figure 9b) along the 2-fold screw axis ($x = 0$, $z = {}^1/_4$ or ${}^3/_4$).

The donor hydrogen atoms closest to the anions orient toward the large cavities surrounded by nitrile groups with the (CN)···H distances of 2.3−2.9 Å, which indicates the presence of donor−anion interaction. Since the molecular orientation of the donor is alternated at $z = {}^1/_4$ and ${}^3/_4$ planes which cross near the center of the anions, this interaction seems to modify the I_3-type arrangement. However, most of the structural features of the I_3 type are still preserved for this HCP type, which can be regarded as a minor modification of the I_3 type.

Crystal Structure of $(BEDO\text{-}TTF)[Q(OH)_2]_2$ (27). The triclinic unit cell of the parameters shown in Table 3 comprises one BEDO-TTF molecule on the center of inversion and two $Q(OH)_2$ ones in the general position. The bond lengths and angles of these molecules are almost identical to those of their respective neutral crystals.[13a,59] The formation of this neutral CT complex accompanies the conformational change of the donor molecule from deformed to planar (except the terminal ethylene groups), as is similarly observed in the formation of several complexes of tetrakis(alkylchalcogeno)-TTF.[60]

(59) Semmingsen, D. *Acta Chem. Scand.* **1977**, *B31*, 11.

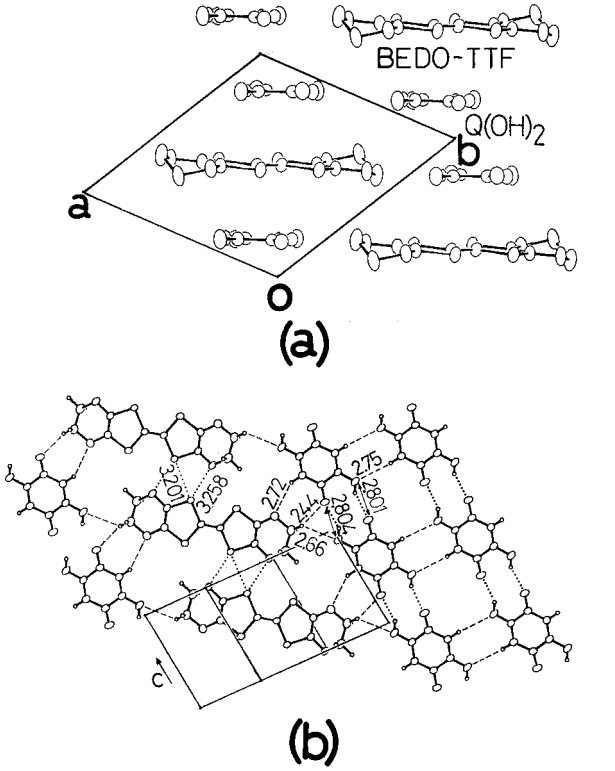

Figure 10. Crystal structures of $(BEDO\text{-}TTF)[Q(OH)_2]_2$ (**27**): (a) crystal structure viewed along the *c* axis; (b) nearly coplanar arrangement of molecules viewed onto the (120) plane. Short O−H···O hydrogen bonds and S···S and S···O contacts are shown by dotted lines. Short C−H···O contacts are shown by broken lines. The distances are shown in angstrom for crystallographically independent contacts.

The complex **27** consists of DAA-type alternating stack along the [110] direction with interplanar separations of 3.4 Å for D−A and 3.2 Å for A−A, accompanied by many intermolecular atomic contacts shorter than the vdW sums. The dihedral angle between molecules is 7.1° for D−A and 0° for A−A.

The (120) plane contains the $Q(OH)_2$ molecules, which are uniformly arranged along the *c* axis (Figure 10b). They are connected by hydrogen bonding between carbonyl and hydroxy groups with the O···O distances of 2.80 Å.

The intermolecular S···S and S···O contacts (dotted lines in Figure 10b) uniformly link donor molecules with each other along the *c* axis. This side-by-side array is similar to that in the neutral BEDO-TTF crystal but different from the arrangement in radical salts (cf., Figure 7d). The S···S distance of 3.20 Å is quite short compared with usual > 3.3 Å, as well as with the distance for the neutral BEDO-TTF crystal (3.5 Å).

The BEDO-TTF molecule has a number of short C−H···O contacts with $Q(OH)_2$ molecules on the same and neighboring (120) planes. The $Q(OH)_2$ molecules tightly linked by hydrogen bonds seem to induce the markedly short intermolecular S···S contacts indirectly through these C−H···O contacts.

Crystal Structure of (BEDO-TTF)(TNBP) (29). The half of the respective molecules are crystallographically independent in the monoclinic unit cell, the parameters of which are given in Table 3. The 2-fold axis crosses the BEDO-TTF molecule along the normal of molecular plane, while the TNBP molecule locates on the center of inversion.

The terminal ethylene groups of the planar donor molecules are disordered, in contrast to the eclipsed conformation in the

(60) Saito, G.; Kumagai, H.; Katayama, C.; Tanaka, C.; Tanaka, J.; Wu, P.; Mori, T.; Imaeda, K.; Enoki, T.; Inokuchi, H.; Higuchi, Y.; Yasuoka, N. *Israel J. Chem.* **1986**, *27*, 319.

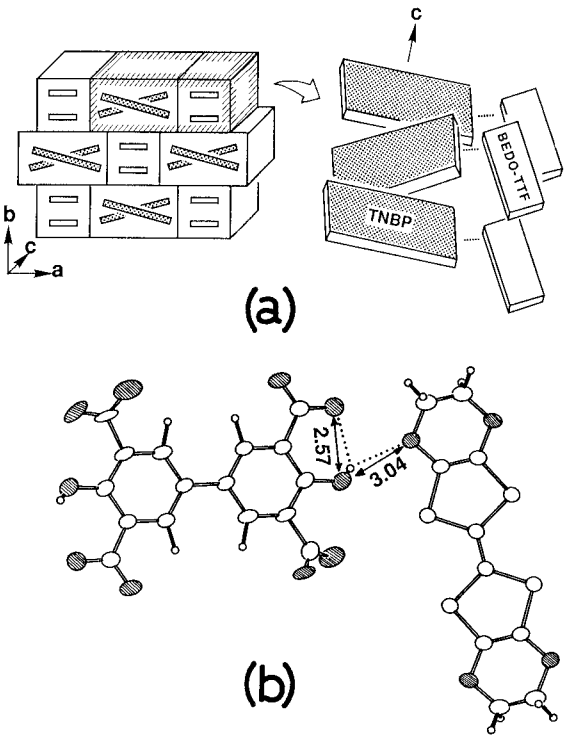

Figure 11. Crystal structures of (BEDO-TTF)(TNBP) (**29**). (a) Schematic representation of molecular packing. The left figure indicates projection approximately along the *c* axis (almost parallel to the molecular plane). A portion is magnified on the right as the projection from the direction oblique to the molecular planes. BEDO-TTF and TNBP molecules are depicted by unshaded and shaded plates, respectively. Intermolecular O—H···O hydrogen bonds are shown by dotted lines. (b) Inter- and intramolecular hydrogen bonds (Å) between donor and acceptor molecules. Oxygen atoms are shaded.

above five BEDO-TTF complexes. This difference can be attributed to the absence of short C—H···O contacts between the donor molecules in this crystal. Of the two crystallographically independent nitro groups of TNBP, one is disordered into two conformations by respective weight of $^1/_2$. Only the oxygen atom of this disordered nitro group deviate from the molecular plane.

The ORTEP drawing and the schematic representation of this crystal structure are illustrated in Figure 11. Both component molecules, which tilt their longitudinal directions by 80° and their planes by 16° with respect to each other, fail to construct columnar structures.

TNBP molecules link to each other at the disordered nitro groups along the *c* axis by short N···O contacts (3.03 Å) with the dihedral angle of 32°. In the light of the steric problem, the disordered nitro group should contact with a differently conformed group of the neighboring molecule.

The most characteristic feature in this crystal is the hydrogen bonds. The hydroxy groups of TNBP form not only intramolecular O-H···O bonds, but also intermolecular bonds using the oxygen of BEDO-TTF (the dotted lines in Figure 11). This suggests that the oxygen atom of this donor possesses a high ability to form intermolecular hydrogen bonds with hydroxy groups of an organic acid.

Donor Packing Pattern in the BEDO-TTF Radical Salts. Including the structural determination in this work, crystal structures have been determined for the 10 BEDO-TTF radical salts summarized in Table 6.[61] All these feature a donor layer with long molecular axes aligned nearly in parallel. The donor-packing patterns in the layer can be classified into only three (the I_3, HCP, and Cl) types, the former two of which have already been mentioned. The most simple array is the I_3 type, which is composed of uniformly packed molecules with their planes parallel to each other. This packing is the major type found in eight salts (**31**, **33**, **34**, I_3, $AuBr_2$, ClO_4, $Cu_2(NCS)_3$, and ReO_4 salts). For the remaining two, the HCP (**37**) and Cl salts,[14e] the molecules are alternated by two stacks (i.e. AA′BB′ type array), and alternated by stack to form herringbone-type arrangement, respectively.

The donor stacking is strictly or almost uniform in each crystal, as evidenced by the marginal variation in crystallographically independent D, δ, and ϵ values (Table 6). The I_3 and HCP types share almost the same stacking parameters ($D \approx 3.5$ Å, $\delta \approx 60°$, $\epsilon \approx 90°$). The donor molecule in the Cl salt shows slipped stacking along its transverse axis ($\epsilon = 92.7°$), having a much smaller δ (43.8°) than other salts.

The short intrastack C—H···O contacts, which have been pointed out to stabilize the stacks in the ClO_4, $AuBr_2$, and $Cu_2(NCS)_3$ salts,[62] are observed in all the BEDO-TTF salts except the Cl salt (Table 6). Some BEDO-TTF salts also show interstack C—H···O contacts.

The interstack arrays in the I_3 and HCP types reveal coplanar linkage of the molecules with two or three S···S and one or two S···O short atomic contacts. Only the Cl salt has no pairs of coplanar molecules.

The above features indicate the strong self-aggregation of BEDO-TTF molecules into the I_3-type array almost regardless of the counter components. This nature is explicitly observed as a severe disorder of the counter components in the two I_3-type salts (**31**, **33**) and a misfit of periodicity between the donor layer and the anion in $(BEDO\text{-}TTF)_{2.4}I_3$.[14a]

In the case of BEDT-TTF salts, the donor packing is determined mainly by the donor—anion interactions,[63,64] which allow the flexible conformation of terminal ethylene groups and various packing patterns depending on the anions. On the other hand, the BEDO-TTF molecule has rigidly fixed terminal ethylene groups and is frequently compelled to stack monotonously. Such contrastive structural features can be attributed to the different electronegativity of the outer heteroatoms (oxygen (3.5) vs sulfur (2.5)). As exemplified by the O—H···O bonds in the complex **29**, strong hydrogen bonding is allowed for the BEDO-TTF, but impossible for the BEDT-TTF. The oxygen atoms in the BEDO-TTF salts afford 2-4 intermolecular C—H···O contacts on the average per molecule (Table 6). The C—H···O contact is often seen in organic crystals and has been known, as the weak hydrogen bond, to play an important role in determining molecular array.[65] Upon oxidation to BEDO-TTF^+, the oxygen atom is considered to remain electronegative because of its little HOMO coefficient (see below). Therefore,

(61) In addition to these 10 salts, the crystal structures of two kinds of $(BEDO\text{-}TTF)_2CF_3SO_3$ salts have been very recently reported. One of these is the first example that reveals κ-type donor packing. The other is of the I_3 type. Fettouhi, M.; Ouahab, L.; Serhani, D.; Fabre, J. M.; Ducasse, L.; Amiell, J.; Canet, R.; Delahés, P. *J. Mater. Chem.* **1993**, *3*, 1101. Also, we have recently obtained crystal structures of fully ionic $(BEDO\text{-}TTF)_2[M(dto)_2]$ (dto = dithiooxalate, M = Ni, Pd) and $(BEDO\text{-}TTF)I_3$. Their structural properties, which are quite different from those of metallic BEDO-TTF salts, are reported elsewhere.[14f,39]

(62) (a) Whangbo, M.-H.; Jung, D.; Ren, J.; Evain, M.; Novoa, J. J.; Mota, F.; Alvarez, S.; Williams, J. M.; Beno, M. A.; Kini, A. M.; Wang, H. H.; Ferraro, J. R. In *The Physics and Chemistry of Organic Superconductors*; Springer, Proceeding in Physics, Vol. 51; Saito, G., Kagoshima, S., Eds.; Springer-Verlag: Berlin, 1990; p 262. (b) Whangbo, M.-H.; Novoa, J. J.; Jung, D.; Williams, J. M.; Kini, A. M.; Wang, H. H.; Geiser, U.; Beno, M. A.; Carlson, K. D. In *Organic Superconductivity*; Kresin, V. Z., Little, A. W., Eds.; Plenum Press: New York, 1990; p 243.

(63) Yamochi, H.; Komatsu, T.; Matsukawa, N.; Saito, G.; Mori, T.; Kusunoki, M.; Sakaguchi, K. *J. Am. Chem. Soc.* **1993**, *115*, 11319.

(64) Whangbo, M.-H.; Williams, J. M.; Schultz, A. J.; Emge, T. J.; Beno, M. A. *J. Am. Chem. Soc.* **1987**, *109*, 90.

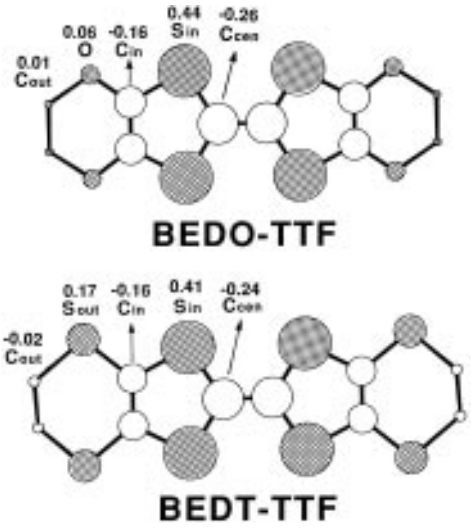

Figure 12. Calculated HOMO coefficients of BEDO-TTF and BEDT-TTF. The magnitude of the coefficient is shown by the radius of the circle.

the C—H···O contacts in the cation salts are also expected to be electrostatic so as to stabilize the donor packing. The geometry of the contacts is a typical one among the known C—H···O hydrogen bonds. For example, **33** shows the intrastack H···O distances of 2.63−2.72 Å, and its C—H···O angles (148−151°) are very close to the mean values of C—H···O angle (152.7°).[65] The sp^3 lone pairs of the oxygen atoms direct approximately toward the hydrogen atoms; the angles of C_{in}—O···H (125−127°) and C_{out}—O···H (91−94°) are close to the idealized lone-pair direction (109.5°) (see Figure 12 for definition of C_{in} and C_{out}). Although the individual energy of the C—H···O bond is small (estimated at 0.6−1.8 kcal/mol),[66,67] this interaction seems to stabilize particularly the I_3-type array due to the large number of the contacts. It should be noted that a sufficiently large number of weak hydrogen bonds between the donor and counter molecules can more or less modify the donor packing. A most typical example is the Cl salt, in which a number of short C—H···O and C—H···Cl contacts with counter components can be regarded as the origin of the different array of the donor.[14e]

Finally notice should be paid to the difference between BEDO-TTF and BEDT-TTF in the side-by-side atomic contacts. For the clarity, S_{in} and S_{out} are defined as the sulfur atoms in TTF moiety and in the six-membered rings of BEDT-TTF, respectively. In the BEDT-TTF salts, the six-membered rings are larger than those of BEDO-TTF so as to prevent the short S_{in}···S_{in} contacts observed in BEDO-TTF complexes. In turn, BEDT-TTF molecules make short S_{in}···S_{out} and S_{out}···S_{out} contacts. As discussed later, S_{in}···S_{in} contacts are highly effective for the increment of the intermolecular overlap integrals, and hence, the pattern of S···S atomic contacts reflects the magnitude of the interstack interactions.

Intermolecular Overlap Integral. In order to examine the relation between the crystal and electronic structures, the band calculations are carried out on all 10 BEDO-TTF salts with known crystal structures. Our calculations, which differ in parameters used from the refs 14c, 15a, and 68, have reproduced qualitatively the same energy dispersions and Fermi surfaces as the reported ones.

In Figure 12, the calculated HOMO of BEDO-TTF based on the molecular structure in **34** is compared with that of BEDT-TTF in the $(BEDT\text{-}TTF)_2ClO_4(TCE)$ salt.[21] Each HOMO has the same symmetry (b_{1u}) and the maximum coefficients on S_{in} atoms. It should be noted that the coefficients on the oxygen atoms in BEDO-TTF are much smaller than those on the S_{out} atoms in BEDT-TTF.

The intermolecular overlap integrals of the BEDO-TTF salts are classified into six types (*p*, *q*, *r*, *s*, *u*, *w*) according to their packing motifes as follows. The I_3-type exhibits three kinds of interactions within a stack (s_i, $i = 1-3$), between stacks along the transverse (p_i, $i = 1-3$), and oblique (q_i, $i = 1-3$) directions (for example see Figure 7a). For the HCP salt (**37**), *s*, *p*, *q* are defined in the same way for the interactions in the stacking pairs AA′ and BB′ whose packing motif is closely related to the I_3 type. An additional interaction in the pairs A′B and B′A is denoted by u (Figure 9a). The intra- and interstack interactions in the Cl salt are labeled differently (*r* and *w*, respectively) from those in the other two types because of the distinct donor packing.

Table 6 summarizes the calculated overlap integrals. The I_3 and HCP types show the same trend in the magnitude of *s*, *p*, and *q*; the intrastack interactions (*s*) are the smallest ($3 \times 10^{-3} < s < 6 \times 10^{-3}$) while the side-by-side ones (*p*) are larger than 10^{-2}, reflecting the multiheteroatom contacts. The oblique interstack interactions (*q*) are as large as the value of *p*, despite the absence of S···S vdW contacts. The 2D semimetal $(BEDT\text{-}TTF)_2(ClO_4)(TCE)_{0.5}$ has been shown to be an example of intrastack interaction being smaller than the interstack ones.[21a] In the HCP salt, the interstack interaction between the nonparallel molecules (*u*) is small compared with those between parallel molecules (*p*, *q*). The Cl salt shows intrastack interaction (*r*) comparable to the interstack one (*w*), although the former is much larger than s_i in other salts.

In all the BEDO-TTF salts, the interstack interactions are found to be significant. The hint to the origin of these interactions was found by the following examination of the relation between of interaction magnitude and the side-by-side atomic contacts. In the radical salts, there are two or three short S···S (≤3.60 Å) and one or two S···O (≤3.32 Å) contacts, which in combination results in the large *p*. For our comparison, we calculated the interactions in the neutral BEDO-TTF and the neutral complexes, (BEDO-TTF) $[Q(OH)_2]_2$ (**27**) and (BEDO-TTF) (TNBP) (**29**). The former two crystals are very similar in side-by-side array, which includes only one short S···S and two S···O contacts. Compared with neutral BEDO-TTF (-1.8×10^{-3}), the very short S···S distance (3.20 Å) in **27** enhances the overlap integral (3.8×10^{-3}), which is, however, much smaller than those in the radical salts ($p_i > 10 \times 10^{-3}$). The interaction between the donor molecules linked by only two S···O contacts in **29** is even smaller (0.2×10^{-3}). These facts indicate that the number of the S_{in}···S_{in} rather than the S_{in}···O contacts is critical for the increment of the side-by-side interactions.

To examine how the heteroatoms of BEDO-TTF contribute to the intermolecular interactions, we calculated the overlap integrals assuming zero coefficients of the HOMO for all the orbitals on the outer ethylenedioxy groups. For example, in $(BEDO\text{-}TTF)_{2.4}I_3$, the magnitude of the overlap integrals ($\times 10^{-3}$) decreases slightly; *s*, 5.5 → 5.3 (−3.1%); *p*, 15.2 → 15.0 (−1.9%); and *q*, 13.0 → 12.6 (−3.4%). Therefore, the

(65) Desiraju, G. R. *Acc. Chem. Res.* **1991**, *24*, 290.
(66) Novoa, J. J.; Tarron, B.; Whangbo, M.-H.; Williams, J. M. *J. Chem. Phys.* **1991**, *95*, 5179.
(67) Seiler, P.; Dunitz, D. D. *Helv. Chim. Acta* **1989**, *72*, 1125.
(68) (a) Cisarova, I.; Maly, K.; Bu, X.; Frost-Jensen, A.; Sommer-Larsen, P.; Coppens, P. *Chem. Mater.* **1991**, *3*, 647. (b) Kahlich, S.; Schweitzer, D.; Rovira, C.; Paradis, J. A.; Whangbo, M.-H.; Heinen, I.; Keller, H. J.; Nuber, B.; Bele, P.; Brunner, H.; Schibaeva, R. P. *Z. Phys. B Condens. Matter* **1994**, *94*, 39.

contribution of the oxygen atoms to the interactions is slight. For comparison, we performed an analogous calculation on β''-(BEDT-TTF)$_2$AuBr$_2$, because of the similar donor arrangement to the I_3 type,[69] and obtained contrastive results with those for BEDO-TTF as follows. Eliminating the HOMO coefficients on the ethylenedithio groups results in a considerable decrease in overlap integrals: ($\times 10^{-3}$) intrastack, 1.5 → 0.2 (−83%), 6.6 → 3.9 (−41%); side-by-side, 8.7 → 5.9 (−32%), 9.6 → 4.4 (−54%); oblique, 15.0 → 11.3 (−25%). This indicates the importance of the S_{out} atoms in the intermolecular interactions of BEDT-TTF.

To account for such a difference between two analogous donors, one must compare their HOMO's (Figure 12). Their features can be summarized as follows: (i) the coefficients on the carbon atoms show little difference between the donors; (ii) larger coefficients are found on the S_{in} atoms (0.44, 0.41) than on the outer heteroatoms [0.06(O), 0.17(S_{out})] for BEDO-TTF and BEDT-TTF, respectively; (iii) the coefficients on the oxygen atoms (0.06) are very small compared to those of on the S_{out} atoms (0.17); (iv) the C_{out} atoms have coefficients of almost zero. From ii, the inner sulfur atoms can be regarded as the most effective for increasing interactions for both donors. Due to iii, the contribution of the oxygen atoms is much smaller than that of the S_{out} atoms of BEDT-TTF, which represents the clear distinction between the two donors.

In addition to the character of the HOMO's, the steric factors must be considered, particularly in the case of the side-by-side interactions. As discussed in the previous section, the smaller six-membered ring enables the closer $S_{in}\cdots S_{in}$ contacts among BEDO-TTF molecules as compared to the BEDT-TTF molecules. Reflecting this, the side-by-side interaction p in the (BEDO-TTF)$_{2.4}$I$_3$ (15.2×10^{-3}) is much larger than the corresponding ones in β''-(BEDT-TTF)$_2$AuBr$_2$ (8.7×10^{-3}, 9.6×10^{-3}).

To summarize the above discussion, the large intermolecular interactions in the BEDO-TTF salts are realized by the sterically allowed close contacts among the inner sulfur atoms with maximum HOMO coefficients.

Band Electronic Structure. The calculated Fermi surfaces, energy dispersions and densities of states (DOS) are shown in Figure 13 for the CF (**33**), HCTMM (**31**), SQA (**34**) and HCP (**37**) salts, respectively. The calculated Fermi surfaces of other known BEDO-TTF salts are shown in Figure 14. Both the **33** and I_3 salt contain only one donor molecule in the respective unit cell to form one HOMO band. The resulting Fermi surfaces are ellipses elongated approximately along the stacking direction where the intermolecular interactions are the weakest (Figures 13a and 14a). For other I_3-type salts containing a large number of donor molecules in the unit cell, the first Brillioun zones (BZs) are folded according to the respective periodicity. While a closed Fermi surface remains unfolded in the $Cu_2(NCS)_3$ salt (Figure 14b), the respective BZs fold the original closed ones, producing closed pockets and/or open Fermi surfaces for the **31**, **34**, ClO_4, $AuBr_2$, and ReO_4 salts (Figures 13b,c and 14c−e). For example, the Fermi surfaces of **31** consist of closed ones centered around the B point and open ones along the k_c direction (Figure 13b). In the case of **34** (Figure 13c), two electron-like and one hole-like pockets are centered around B, Z, and X points, respectively. Table 6 summarizes the respective area ratios of the closed Fermi surfaces to the BZ (S_{FS}/S_{BZ}), the density of states at the Fermi level $N(E_F)$, and band width. With the exception of the $AuBr_2$ salt with 1D character, all I_3-type salts show 2D Fermi surfaces. The Fermi surface of the Cl salt is close to forming a circle, which phenomenon arises from almost the isotropic intermolecular overlap within a donor layer (Figure 14f).[70] The 2D nature is supported by the nearly isotropic conductivities in the layer for **31** ($\sigma_{a+2c}/\sigma_{2a-c} = 0.4$) and ReO_4 salt[68b] ($\sigma_a^*/\sigma_c = 1/3$). Also, for the ReO_4 and Cl salts, the recent observations of the Shubnikov−de Haas effect[68b,71] confirm the existence of the closed Fermi surfaces. It is thus concluded that BEDO-TTF tends to form a 2D electronic structure due to the large interstack interactions, *p*, *q* and *w*.

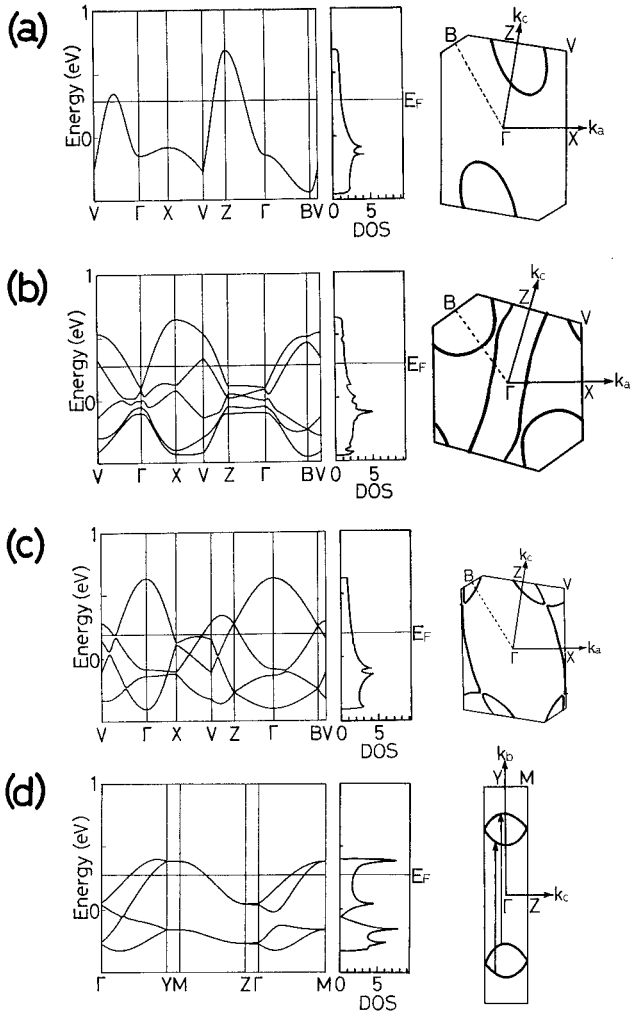

Figure 13. Calculated band structures, densities of states (DOSs), and Fermi surfaces of (a) (BEDO-TTF)$_{10}$(CF)$_4$(H$_2$O)$_3$ (**33**), (b) (BEDO-TTF)$_5$(HCTMM)(PhCN)$_2$ (**31**), (c) (BEDO-TTF)$_4$(SQA)(H$_2$O)$_6$ (**34**), and (d) (BEDO-TTF)$_5$(HCP)(PhCN)$_{0.2}$ (**37**). The DOSs are given in states(total)/(eV molecule of BEDO-TTF). The nesting vector **q** is represented by arrows in d.

The semiconducting (BEDO-TTF)$_5$(HCP)(PhCN)$_{0.2}$ (**37**) shows four HOMO bands, which are much more dispersive along the *b** than along the *c** axis (Figure 13d). The energy band at the ZM zone boundary is degenerate due to the existence of the *c* glide plane. The Fermi level determined by $\gamma = 0.40$ cuts the upper two bands along the *b** direction. The resulted Fermi surfaces are open and very similar to those of α″-(BEDT-

(69) Mori, T.; Sakai, F.; Saito, G.; Inokuchi, H. *Chem. Lett.* **1986**, 1037.

(70) The authors in ref 14e described the stoichiometry as (BEDO-TTF)-Cl(H$_2$O). However, Mori et al. showed the stoichiometry as (BEDO-TTF)$_2$-Cl(H$_2$O)$_3$ on the basis of the Shubnikov−de Haas and de Haas−van Alphen effects.[71] Our elemental analysis (±0.3% for C, H, and O) and measurement of the density of this salt also confirm the latter result ($\varrho_{obs} = \varrho_{calc} = 1.73$ vs $\varrho_{calc} = 1.77$ for 1:1:1 stoichiometry). Accordingly, the $^3/_4$-filling was adopted for our calculation.

(71) Mori, T.; Oshima, K.; Okuno, H.; Kato, K.; Mori, H.; Tanaka, S. *Phys. Rev. B* **1995**, *51*, 11110.

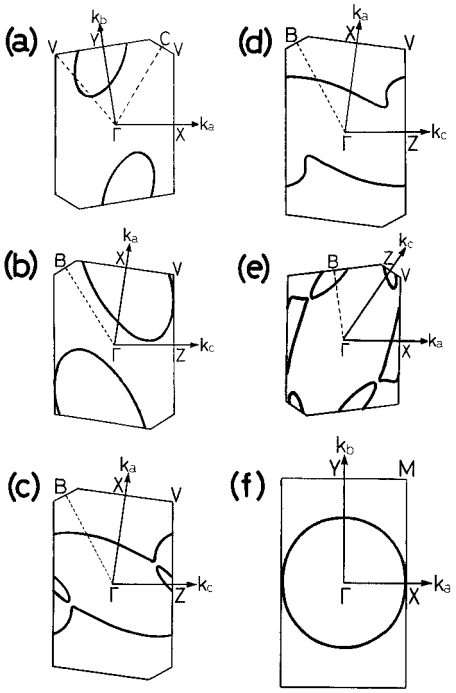

Figure 14. Calculated Fermi surfaces of (a) $(BEDO\text{-}TTF)_{2.4}I_3$, (b) $(BEDO\text{-}TTF)_3Cu_2(NCS)_3$, (c) $(BEDO\text{-}TTF)_2ClO_4$, (d) $(BEDO\text{-}TTF)_2AuBr_2$, (e) $(BEDO\text{-}TTF)_2ReO_4(H_2O)$, and (f) $(BEDO\text{-}TTF)_2Cl(H_2O)_3$.

$TTF)_2CsHg(SCN)_4$, as is the donor packing.[58] The two Fermi surfaces are well superposed to each other by translation vector **q** ($= {}^3/_5b^*$) (arrows in Figure 13d). The nesting of the Fermi surfaces, which is often seen in the quasi-1D materials, typically causes the CDW- or SDW-associated metal−insulator transition. As mentioned above, the anion arrangement in **37** is considered to give the superlattice of (a, $5b$, c), which corresponds to the vector **q**. Although the structural analysis assumes a uniform donor stack, the periodicity of the anions should distort the stack more or less through the electrostatic interaction in the actual crystal. With a little periodic potential on the stack, the electronic system can gain large stabilization energy due to the almost perfect nesting and the larger $N(E_F)$ as compared to other BEDO-TTF salts (Table 6). This is the most plausible reason for the semiconducting nature of **37**.

Next we will see the density of states (DOS) in the above nine metallic BEDO-TTF salts. The shapes of Fermi surfaces and band fillings vary with salts, but, following common features, can be seen in the DOSs of the HOMO bands: (i) Their total bands have no energy gaps, owing to the nearly uniform donor packing. (ii) Their widths (0.9−1.2 eV) are little dependent on the salts. (iii) The DOS's are almost independent on the energy in their upper region where the Fermi level lies, and the maximum peaks appear in the lower region. These similarities can be attributed to the similar donor arrangements and intermolecular interactions. It should also be noted that the $N(E_F)$ values are almost independent on the salts (Table 6).

Finally, we will discuss the relation between the conducting properties and the DOS of BEDO-TTF salts. The higher superconducting transition temperature (T_c) is often found to be originated from the larger $N(E_F)$. In the case of BEDT-TTF-based superconductors, T_c values have been found to be proportional to the volume of the space of the delocalized carriers, which should be related to the $N(E_F)$.[63] On the other hand, the narrower band width enhances the effective mass of conduction electrons. Therefore, poor conductivity is generally expected in the salts with large $N(E_F)$, assuming equivalent relaxation time and concentrations of carriers. It is interesting to note that the $N(E_F)$ values of the superconducting $Cu_2(NCS)_3$ and ReO_4 salts ($T_c \sim 1$ K) are the largest [1.46 states(total)/(eV molecule)] among the metallic BEDO-TTF salts. These values are, however, much smaller than those of κ-$(BEDT\text{-}TTF)_2X$ salts (X = $Cu(NCS)_2$, $Cu[N(CN)_2]Br$, $Cu(CN)[N(CN)_2]$) with high T_c (10−13 K) [$N(E_F) = 1.8-2.1$ states(total)/(eV molecule)].[63,72] Such low $N(E_F)$ may be one of the reasons why the T_c of the BEDO-TTF salts are very low. Conversely, concerning the σ_{rt} values, BEDO-TTF (70−200 S cm^{-1}) is superior to the above κ-$(BEDT\text{-}TTF)_2X$ salts (40−50 S cm^{-1}), which concurs with the above expectation. Therefore, one should increase $N(E_F)$ to obtain the BEDO-TTF salts with higher T_c. To meet this requirement, two methods can be proposed; one is the reduction of the intermolecular overlap integrals by modification of the molecular array, and the other is the control of the γ value. However, the former seems rather difficult since BEDO-TTF tends to form the same (I_3-type) array independently on the anions. Considering the energy dependence of the DOS of the above BEDO-TTF salts, increasing γ and hence lowering the Fermi level will raise the $N(E_F)$; $\gamma = 1.1-1.3$ corresponds to the maximal $N(E_F)$. To put it another way, further oxidation is needed for higher T_c.

Origin of Metallic Behavior of BEDO-TTF Complexes. Here we discuss the origin of the metallic behavior of BEDO-TTF complexes from a molecular point of view. One of the important features of the BEDO-TTF radical salts is the self-assembled layered structure of the donor molecule. Such a layered structure is essential, but alone is not sufficient for the 2D electronic structure which will suppress the Peierls transition and stabilize the metallic state to the low temperature. In the I_3 type, two kinds of large interstack interactions (p and q) of almost the same magnitude are crucial for 2D. Although BEDO-TTF is analogous to BEDT-TTF, their 2D nature is realized in different ways. The outer heteroatoms directly contribute to the increment of the interstack interactions in the BEDT-TTF compounds, but not in the BEDO-TTF. Instead, the oxygen atoms of a BEDO-TTF molecule play two kinds of indirect roles in fabricating the 2D electronic structure. The first role is that the small oxygen atoms allow close contacts among the inner sulfur atoms sterically, and consequently enhance the intermolecular overlap. The second is that the electronegative oxygen atoms drive the molecules to assemble into the I_3-type array via the C−H···O interactions, so that a higher dimensional electronic structure is achieved.

Another important characteristic of the BEDO-TTF complexes is their wide band width, which is also the stabilizing factor of the metallic state. In the case of organic metals of TTF-TCNQ system, most are 1D so that the band width is described simply by $4t$ where t is the transfer integral. The overlap integral (S) of the TTF derivatives (excluding Se derivatives) maximizes when the molecules overlap in a face-to-face eclipsed manner.[21a] In this case, S is at most 25×10^{-3}, and thus the band width is narrower than 1 eV using $t = -ES$ where $E = -10$ eV. Although the individual overlap integrals are much smaller than 25×10^{-3} in the BEDO-TTF complexes, the calculated total bands in the I_3 and Cl types have as large widths as 0.9−1.2 eV, owing to 2D interactions. In the case of BEDT-TTF salts, strong dimerization of the donor molecules frequently splits the HOMO bands and sometimes leads to the Mott insulator.[73] For BEDO-TTF salts, on the other hand, the almost uniform array of the donor molecules prevents an opening of the energy gap in the HOMO bands.

(72) The $N(E_F)$ values of the κ-$(BEDT\text{-}TTF)_2X$ salts were calculated on the basis of the same parameters as in this work. $N(E_F) = 1.90$ states-(total)/(eV molecule) was obtained for the X = $Cu[N(CN)_2]Br$ salt by utilizing its structural data.[10b]

Conclusion

This work has demonstrated the peculiar ability of BEDO-TTF to produce wide variety of organic metals independent of the size, shape, and electronic structures of their counter components. Furthermore, the metallic state of these BEDO-TTF complexes is often stable to low temperatures (<20 K). This donor provides a number of organic metals with smaller degree of CT ($\gamma \geq 0.3$) and from combination with much weaker acceptors ($\Delta E^{o,r} \leq 0.57$ V) than expected with conventional TTF-TCNQ system organic metals ($\gamma \geq 0.5$, -0.02 V $\leq \Delta E^{o,r} \leq 0.34$ V). Another unique characteristic of the metallic complexes is their excess content of BEDO-TTF, which allows the partial CT ground state in the complexes with strong acceptor molecules.

In the crystal structures of metallic BEDO-TTF complexes, donor molecules aggregate to form a layered structure and usually construct uniform (I_3-type) array connected by intrastack C—H···O and side-by-side heteroatom short contacts. Most metallic BEDO-TTF complexes show 2D band electronic structures and relatively wide band width due to two kinds of strong interstack interactions. The unusually easy access to organic metals is attributable to a strong trend in the structural properties of BEDO-TTF. We also noted that the $N(E_F)$ of these metallic salts are much lower than in the superconducting BEDT-TTF salts having higher T_c. In this respect, higher γ will be needed to produce a higher T_c BEDO-TTF superconductor.

The sulfur atoms (S_{in}) are dominant for intermolecular orbital overlap, while the smaller oxygen atoms not only enhance side-by-side $S_{in}\cdots S_{in}$ contacts, but also stabilize the self-aggregated structure of BEDO-TTF molecules through weak hydrogen bonding. From these facts we can conclude that the shape and electronic state of BEDO-TTF are very suitable for 2D band structure, resulting in a stable metallic state. This donor molecule is expected to open the way to numerous systematic studies on the 2D conducting system by introducing various counter components (e.g. magnetic anions) and/or disorder without changing the donor arrangement in metallic BEDO-TTF layers.

Acknowledgment. The authors thank Dr. Takehiko Mori for providing his calculating program used in this band structure calculation. We are grateful to Prof. Kazuhiro Nakasuji and Prof. Takayoshi Nakamura, who offered some acceptors, and Dr. Tatsuo Hasegawa for his kind advice for the synthesis of F_2TCNQ and FTCNQ. Also we acknowledge Prof. Takamasa Momose and Prof. Tadamasa Shida for the use of the high-resolution IR spectrometer. This work was supported by a Grant-in-Aid for Science Research from the Ministry of Education, Science, Sports, and Culture, Japan, and a Grant for the Proposal-Based Advanced Industrial Technology R&D Program from NEDO, Japan.

Supporting Information Available: Tables of final atom positions and isotropic thermal parameters for $(BEDO\text{-}TTF)_5(HCTMM)(PhCN)_2$ (**31**) (Table X1), $(BEDO\text{-}TTF)_{10}(CF)_4(H_2O)_3$ (**33**) (Table X2), $(BEDO\text{-}TTF)_4(SQA)(H_2O)_6$ (**34**) (Table X3), $(BEDO\text{-}TTF)_5(HCP)(PhCN)_{0.2}$ (**37**) (Table X4), $(BEDO\text{-}TTF)[Q(OH)_2]_2$ (**27**) (Table X5), (BEDO-TTF)(TNBP) (**29**) (Table X6) and their respective bond lengths and angles (Figure S1−6), and a table of the results of the elemental analysis of all the BEDO-TTF complexes (Table X7) prepared in this work (11 pages). See any current masthead page for ordering and Internet access instructions.

JA960393V

(73) (a) Beno, M. A.; Firestone, M. A.; Leung, P. C. W.; Sowa, L. M.; Wang, H. H.; Williams, J. M.; Whangbo, M.-H. *Solid State Commun*. **1986**, *57*, 735. (b) Obertelli, S. D.; Friend, R. H.; Talham, D. R.; Kurmoo, M.; Day, P. *J. Phys. Condens. Matter*. **1989**, *1*, 5671. (c) Parker, I. D.; Friend, R. H.; Kurmoo, M.; Day, P. *J. Phys. Condens. Matter* **1989**, *1*, 5681. (d) Kinoshita, N.; Tokumoto, M.; Anzai, H.; Saito, G. *Synth. Met.* **1987**, *19*, 203. (e) Tokumoto, M.; Anzai, H.; Ishiguro, T.; Saito, G.; Kobayashi, H.; Kato, R.; Kobayashi, A. *Synth. Met.* **1987**, *19*, 215. (f) Iwasa, Y.; Mizuhashi, K.; Koda, T.; Tokura, Y.; Saito, G. *Phys. Rev. B* **1994**, *49*, 3580. (g) Komatsu, T.; Sato, H.; Nakamura, T.; Matsukawa, N.; Yamochi, H.; Saito, G.; Kusunoki, M.; Sakaguchi, K.; Kagoshima, S. *Bull. Chem. Soc. Jpn.* **1995**, *68*, 2233. (h) Komatsu, T.; Matsukawa, N.; Inoue, T.; Saito, G. *J. Phys. Soc. Jpn.* **1996**, *65*, 1340.